CHOLERA TOXIN SUBUNIT B-MEDIATED INTRACELLULAR TRAFFICKING OF MESOPOROUS SILICA NANOPARTICLES TOWARD THE ENDOPLASMIC RETICULUM

by

William Andrew Walker

A thesis submitted to the faculty of
The University of North Carolina at Charlotte
in partial fulfillment of the requirements
for the degree of Master of Science in
Chemistry

Charlotte

2015

Approved by:

_____
Dr. Didier Dréau

_____
Dr. Jerry Troutman

_____
Dr. Joanna Krueger

_____
Dr. Juan Vivero-Escoto

ABSTRACT

WILLIAM ANDREW WALKER. Cholera toxin subunit B-mediated intracellular trafficking of mesoporous silica nanoparticles toward the endoplasmic reticulum. (Under the direction of DR. JUAN L. VIVERO-ESCOTO)

In recent decades, pharmaceutical research has led to the development of numerous treatments for human disease. Nanoscale delivery systems have the potential to maximize therapeutic outcomes by enabling target specific delivery of these therapeutics. The intracellular localization of many of these materials however, is poorly controlled, leading to sequestration in degradative cellular pathways and limiting the efficacy of their payloads. Numerous proteins, particularly bacterial toxins, have evolved mechanisms to subvert the degradative mechanisms of the cell. Here, we have investigated a possible strategy for shunting intracellular delivery of encapsulated cargoes from these pathways by modifying mesoporous silica nanoparticles (MSNs) with the well-characterized bacterial toxin Cholera toxin subunit B (CTxB). Using established optical imaging methods we investigated the internalization, trafficking, and subcellular localization of our modified MSNs in an *in vitro* animal cell model. We then attempted to demonstrate the practical utility of this approach by using CTxB-modified mesoporous silica nanoparticles to deliver propidium iodide, a membrane-impermeant fluorophore.

DEDICATION

This work, all that has come before and all that might follow is wholly dedicated to my family. To my parents, who first introduced me to the wonders of the natural world and whose constant encouragement has carried me to the place I am today. To my sister and brother, for their unfailing support and uncritical ear. And to my extended family, for always believing in me, regardless of circumstance.

It is also dedicated to all of those over the years who have mentored me as a scientist; to Mrs. Fox and Mrs. Morgan who lead me to discover my passion for the sciences; to Dr. Amy Grunden and Dr. Jon Olson of North Carolina State University for giving me my start in research; and to Dr. Jennifer Miller of North Carolina State University who taught me to observe the highest standards in research.

Special thanks also to my peers, the graduate students of the Departments of Chemistry and Nanoscale Science, without whose support the completion of this work would have been impossible.

ACKNOWLEDGEMENTS

I would like to thank, first and foremost, Dr. Dider Dréau (Department of Biological Sciences, UNC Charlotte) for his assistance in designing and conducting the major aspects of this work. Dr. Joanna Krueger and Dr. Jerry Troutman who, along with Dr. Dréau provided invaluable guidance as a member of my thesis committee. Mr. Amir Hashemi for his assistance with the synthetic aspects of this work. Dr. Thomas Walsh for his generous financial support of my education. And finally, my advisor, Dr. Vivero-Escoto for his support in planning and conducting this work.

TABLE OF CONTENTS

LIST OF ABBREVIATIONS

APTES	aminopropyltriethoxysilane
BET	Braun-Emmett-Teller
CAVME	caveolae-mediated endocytosis
CME	clathrin-mediated endocytosis
CTAB	cetyltrimethylammonium bromide
CTxB	cholera toxin subunit B
DCM	dichloromethane
DLS	dynamic light scattering
DMAP	4-dimethylaminopyridine
EDC	1-ethyl-3-(-3-dimethylaminopropyl) carbodiimide
FACS	Fluorescence-activated cell sorting (flow cytometry)
FTIR	Fourier transform infrared spectroscopy
LSCM	laser scanning confocal microscopy
MPC	macropinocytosis
MSN	Mesoporous Silica Nanoparticle
NMR	nuclear magnetic resonance
PEG	poly(ethylene) glycol
PI	propidium iodide
PPMP	1-phenyl-2-hexa-decanoylamino-3-morpholino-1-propanol
TEM	transmission electron microscopy

TEOS	tetraethyl orthosilicate
TFA	trifluoroacetic acid
TGA	thermogravimetric analysis
THF	tetrahydrofuran

CHAPTER 1: INTRODUCTION

1.1 Emergence of Nanomedicine

Current pharmacological practice is centered on the use of compounds that, while capable of eliciting their therapeutic effects, exhibit limited clinical efficacy due to side effects incurred by their use.[1] These side effects arise primarily from the nonspecific means by which these compounds are introduced to the body and localized to their target tissues.[2] Since many of these compounds lack the ability to specifically localize to their cellular targets, nonspecific uptake by other tissues may occur leading to the aforementioned undesirable side effects. Furthermore, the means of introducing these therapeutic compounds ensures that some amount will be eliminated and/or degraded by the body prior to reaching their designated cellular target, thereby further limiting their therapeutic outcome.[3] Maximizing the benefit of current molecular therapeutics requires that nonspecific side effects be either reduced or eliminated altogether while retaining their beneficial effects. It was the desire to achieve this end that established the discipline of nanomedicine; the use of nanometer scale materials for biomedical technologies and applications. These materials provide a potential avenue by which to overcome the limitations associated with current molecular therapies. Nanoscale drug delivery systems (DDS) provide a means by which to achieve specific targeting and delivery of therapeutic compounds to their target tissue while protecting them from the degradative mechanisms

of the body, minimizing any loss of the compound that may occur prior to reaching its cellular target.[4]

1.2 Nanomaterials as Delivery Systems

Several different materials have been investigated for use as drug delivery systems. Liposomes were among the first and foremost of these, having been shown to improve clinical outcomes of chemotherapeutic treatment associated with certain cancers. Since the introduction of Doxil, the first FDA-approved nanocarrier-based therapeutic agent, fourteen other liposomal formulations have been introduced for the delivery of compounds ranging from antimicrobials to analgesics.[5] Despite their recent success, liposomal materials only partially address the aforementioned problems associated with modern pharmacological therapies. Liposome delivery systems have been shown to suffer from poor *in vivo* stability, leading to premature release by leaking of their therapeutic payloads prior to reaching their cellular targets. This, in addition to the poor release kinetics of liposome-encapsulated molecules, has limited their clinical efficacy.[6] Inorganic nanomaterials have been investigated as a means of addressing the problematic stability that has plagued these more established delivery systems. These materials, particularly plasmonic materials and metal oxides, have the added benefit of possessing well-established chemistries and material-specific properties that make them attractive candidates for multifunctional biomedical materials.[7]

1.3 Mesoporous Silica Materials

Of these materials, mesoporous silica-based nanoparticles have shown exceptional promise for biomedical applications due to their facile synthesis, versatile chemistry, ordered porous structure, and biological inertness.[8] Although MSNs have been

shown to improve the delivery of therapeutic cargoes over conventional methods, significant issues remain to be addressed if this material is to be used as an effective drug delivery system in a clinical setting.

1.4 Interactions of Nanomaterials with their Cellular Targets

1.4.1 Cellular Endocytosis Mechanisms

All cellular life is sustained by the uptake of nutrients from their immediate environment. Consequently, organisms have evolved numerous mechanisms to mediate the translocation of objects ranging from small molecules to macromolecular assemblies across the plasma membrane from the extracellular milieu to the intracellular environment. The pathways used by the cell for the uptake of any given object depend on its physical and chemical properties as well as the genetic makeup of the cell itself.[9] Physical properties such as size, morphology, and surface charge (or lack thereof) have been shown to dictate the biological mechanisms used by the cell for the uptake of exogenous materials.[4] The presence or absence of certain chemical structures can also play a part in material uptake by the cell through the interaction of these groups with specific cellular receptors. These interactions may be nonspecific, permitting the internalization of a wide range of materials by the cell, or exhibit a high degree of specificity, mediated by unique target-receptor interactions. Recent evidence suggests that the pathway used by the cell for the internalization of a given material plays a significant role in its intracellular fate.[10] For target-specific delivery applications, it then becomes important to tailor the physiochemical composition of nanocarriers to achieve interactions with their cellular targets that are both predictable and favorable. The biological mechanisms used by eukaryotic cells for the uptake of exogenous materials

include numerous endocytotic pathways (Figure 1). Of these, only a handful are well understood with all the others being either poorly characterized or, as of now, undiscovered. These endocytic mechanisms can be broadly categorized as either macroscale or microscale pathways dependent upon the size of the object being engulfed by the cell.[11] Macroscale endocytic pathways, which include phagocytosis and macropinocytosis, generally mediate the internalization of materials greater than 500nm in diameter. With nanoscale materials often regarded as those with sizes less than 100nm, it is microscale and not macroscale endocytic pathways that are most relevant to the uptake of these materials. Of these pathways, clathrin-mediated and caveolae-mediated endocytosis remain the best understood, although the mechanisms of numerous others including CLIC/GEEC, AFR6-dependent, and flotillin-dependent pathways are currently being elucidated.[12]

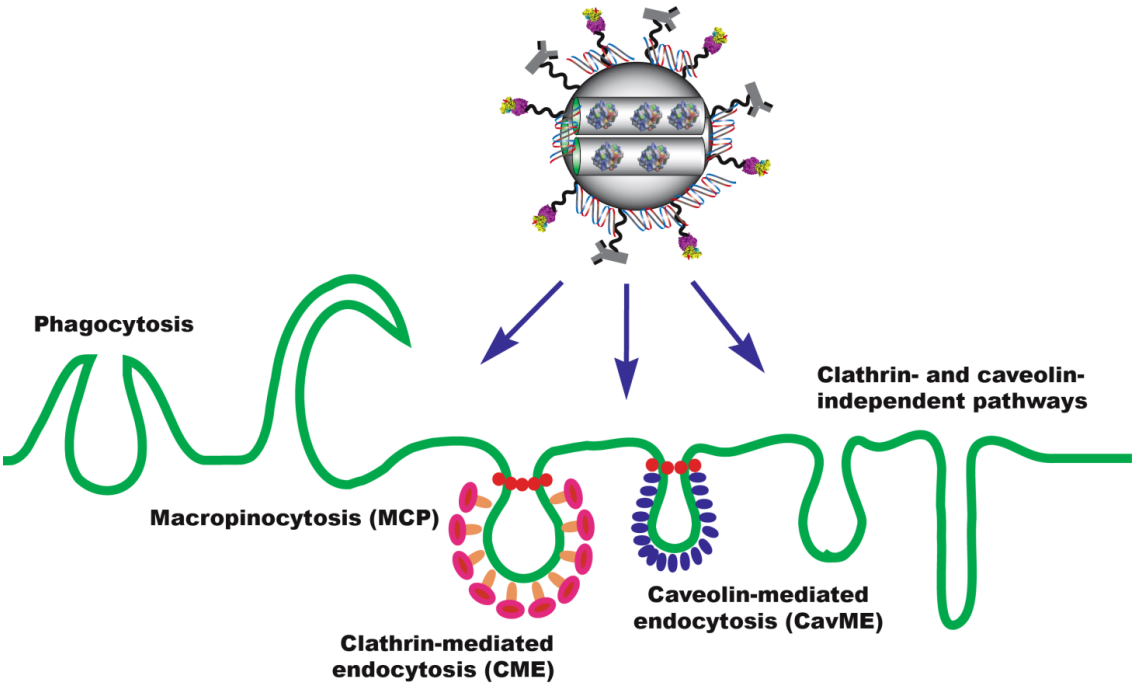

Figure 1.Schematic representation of the different endocytic pathways that can be used by cells for the uptake of nanomaterials.

1.4.2 Intracellular Fate

Cellular life depends on the complex interplay of innumerable biomolecular processes. Among the most complex of these are the mechanisms by which the cell moves components between different cellular organelles and to and from the interior of the cell and its external environment. This is carried out by cellular endosomes bearing molecular signatures whose interactions with motor proteins guide their subsequent trafficking between the different subcellular compartments.[13] The most fundamental of these trafficking patterns, classical or anterograde trafficking, has proteins synthesized in the endoplasmic reticulum surrounding the nucleus moving to the Golgi apparatus. Here, they are further modified in accordance to their designated function and sorted for trafficking from the Golgi apparatus to the plasma membrane or other cellular organelles.[14] Following uptake from the extracellular environment, exogenous materials are subsequently trafficked by the cells through endosomes to different subcellular organelles for further processing. In accordance to mechanisms used by the cell for the movement of endogenous cellular components, the trafficking and ultimate subcellular localization of different exogenous materials is dependent upon the interaction of the material with the surface of the cell.[15] The interaction of the materials surface with the specific receptors and ligands present at the plasma membrane determines the pattern of intracellular trafficking that is followed. For most exogenous components, uptake from the extracellular environment is followed by degradation in lysosomes, releasing the monomeric components of the degraded biomolecules as raw materials for the normal metabolic processes of the cell.[16] The final intracellular localization of nanocarriers has a significant impact on the delivery of molecular therapeutics and their resulting efficacy.

If a material is retained within its target cell in a structure or region isolated from where its cargo is designed to act, reduced therapeutic outcomes may result. With the intracellular fate being dependent on the chemical and physical properties of the material, it then becomes imperative that they be tuned in such a way that they achieve an intracellular localization that maximizes the effect of its therapeutic cargo and avoids those that would serve to limit its effectiveness.

1.5 Issues of Nanomaterial Delivery Systems

One serious limitation to using nanomaterials for molecular delivery is the tendency of nanomaterial-based delivery systems to become entrapped in lysosomes, the degradative organelles of the cell, following uptake by their target cells.[17,18] Entrapment in this organelle prevents delivered therapeutics from reaching their intended targets and places limitations on efficacy of nanomaterial-based therapies. This interaction between nanomaterials and their cellular targets also poses a unique challenge for the delivery of therapeutic biomolecules, which are effectively degraded by the harsh environment of the lysosome.[19,20] New strategies are necessary to make possible the efficient delivery of these and other molecular cargoes to their respective cellular targets.

1.6 Biomolecules as a Means of Altering Cell/Material Interactions

Several different biomolecules, particularly biological toxins, have demonstrated the ability to escape degradation by exploiting alternative modes of intracellular trafficking following internalization by the cell. Among the best characterized of these toxins is the cholera toxin secreted by the aquatic bacterial pathogen *Vibrio cholera*. As a classic AB toxin, cholera toxin has been demonstrated to translocate from the plasma membrane to the endoplasmic reticulum in a retrograde fashion mediated exclusively by

the B subunit of the native holotoxin.[21] Conjugation of biomolecules such as cell penetrating peptides and cellular recognition signals to nanocarriers has been shown to bestow these materials with novel properties such as endosomal escape and organelle-specific localization.[22] Despite the obvious utility of such an approach, investigations into using bacterial toxins and other whole proteins to direct the intracellular localization of nanocarriers are sparse. Chakraborty et al. demonstrated that covalent modification of quantum dots with Cholera toxin subunit B influenced their uptake and intracellular retention.[23] While illustrating the possibility of using such proteins to influence the behavior of nanomaterials, this work fails to provide an in-depth investigation of the effect of CTxB conjugation on nanomaterial uptake and intracellular localization or demonstrate the utility of such an approach for the delivery of molecular therapeutics.

1.7 Research Objective

The intent of this research is to provide evidence of the practical utility of using these proteins to direct the subcellular localization of nanomaterials for delivery applications through the modification of porous silica nanocarriers with CTxB (Figure 2). This work provides an alternative strategy for the development of drug delivery systems capable of intracellular delivery of biomolecules and other sensitive molecular cargoes in a target-specific manner. The following is a brief introduction of the four research objectives that were undertaken to demonstrate this end.

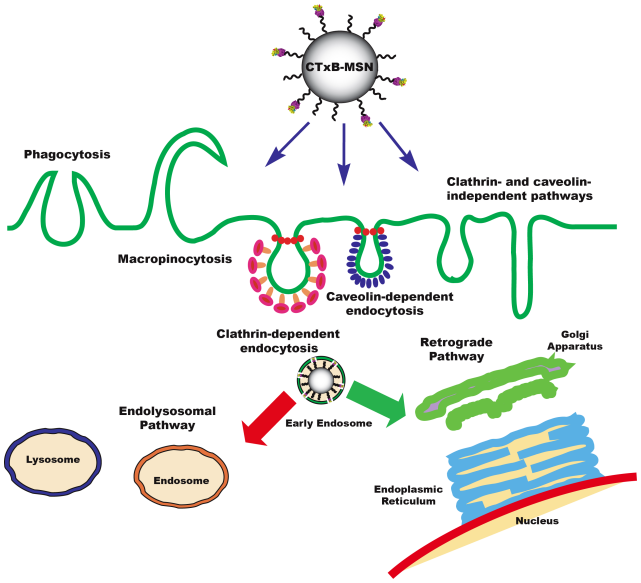

Figure 2. Schematic representation of possible uptake and intracellular localization pathways of CTxB-modifed MSNs.

1.7.1 Synthesis and Characterization of Cholera Toxin Subunit B-Modified Mesoporous Silica Nanoparticles

To demonstrate the effects of toxin conjugation on the interactions between nanomaterials and their cellular targets, model mesoporous delivery systems were synthesized and subsequently modified to bear the CTxB protein (Figure 3). The mesoporous silica materials were synthesized using methods adapted from the literature. A polymeric linker based on poly(ethylene) glycol was then synthesized and grafted to each of these materials. Carbamide bioconjugation chemistry was then used to attach the CTxB protein via the PEG linker to the surface of silica nanomaterials.

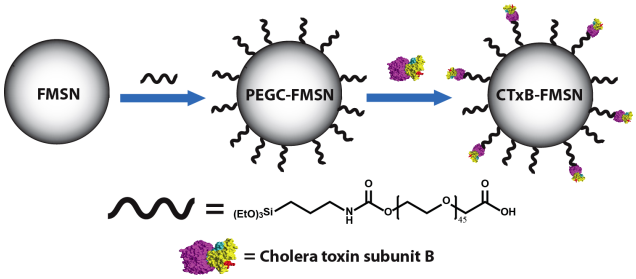

Figure 3. Schematic representation of synthesis of CTxB-MSN materials.

1.7.2 *In Vitro* Internalization of Cholera Toxin Subunit B-Modified Mesoporous Silica Nanoparticles

Several different endocytic pathways mediate the uptake of exogenous materials by cells. The pathways that play a role in the internalization of a given material are determined by its physiochemical properties and, to a degree, the genetic composition of the cell. This means that certain pathways tend to dominate the uptake of similar materials with the extent of this effect varying with the identity of the cell. The pathways that mediate the uptake of a material have also been found to play a role in determining its subcellular localization and intracellular fate. It becomes important then to determine how cellular uptake changes as a consequence of changes in physiochemical properties of the materials. Pharmacological inhibitors were used to evaluate the pathways that play a role in the uptake of porous silica nanomaterials and how these change with subsequent modification of CTxB.

1.7.3 *In Vitro* Subcellular Localization of Cholera Toxin Subunit B-Modified Mesoporous Silica Nanoparticles

Just as the physiochemical properties of a material play a role in its internalization, they can also determine its subsequent subcellular localization. Unlike most nanomaterials, retrograde trafficking bacterial toxins such as Cholera toxin exhibit a characteristic subcellular localization upon entry into the cell. It then becomes important to determine how the intracellular behavior of these materials changes following modification with CTxB. This was accomplished by evaluating colocalization of nanomaterials with selectively labeled cellular organelles using laser scanning confocal

microscopy. The effects of modifying nanomaterials with Cholera toxin could then be quantitatively evaluated.

1.7.4 Demonstration of *In Vitro* Molecular Delivery Using Cholera Toxin Subunit B-Modified Mesoporous Silica Nanoparticles

To exhibit the potential of modifying nanomaterial delivery systems with retrograde trafficking proteins such as CTxB, mesoporous silica nanoparticles modified with CTxB were used to deliver the small fluorescent molecule propidium iodide. As a membrane-impermeant fluorophore that specifically labels double-stranded nucleic acids, propidium iodide can only label viable cells if it is efficiently delivered to the nucleus of its cellular target. Using LSCM, we will evaluate the ability of cholera-toxin modified materials to effectively deliver this fluorescent molecule to its intended subcellular target.

CHAPTER 2: EXPERIMENTAL

2.1 Synthesis of Mesoporous Silica Nanoparticles

Fluorescein-labeled monodisperse mesoporous silica nanoparticles were synthesized using a method adapted from the literature.[24] Briefly, to 21.6 mL of DI H_2O was added 2.7g of ethanol (EtOH); 0.78 g cetyltrimethylammonium bromide (CTAB), and 0.045g diethanolamine (DEA). The resulting solution was stirred vigorously at 60^{o}C for 30min. Consequently, fluorescein isothiocynate (FITC) was added at a 1:1 molar ratio to a 200μL solution of acetonitrile containing aminopropyl triethoxysilane (APTES) and stirred at room temperature under dark conditions for 15-20min. To the first solution was added 2.19 mL of tetramethylorthosilicate (TMOS) dropwise over a period of 5min. Midway through the addition of TMOS, 90μL FITC-labeled APTES was added. The resulting suspension was stirred for an additional 18h at 60^{o}C before being collected by centrifugation and resuspended in EtOH. The surfactant template was removed from the as-synthesized nanoparticles by washing in 1.0M HCl solution in methanol at 60^{o}C with constant stirring for 48h.

2.2 Synthesis of Poly(ethylene) glycol Polymer Linker

A bifunctional PEG linker (Scheme 1) was synthesized using a three-step approach modified from the literature.[25] In the first step, dehydrated poly(ethylene glycol) 2K (PEG 2K; 3mmol; 6g) was dissolved in dry THF (300mL) under N_2 to which was added sodium hydride (NaH ; 9 mmol; 363.3mg). The solution was stirred at RT for

30 min, after which tert-butyl Bromoacetate (tBBA; 7.5 mmol; 1.1 mL) was added and solution stirred for further 24h under N_2 at RT. The products were concentrated by rotary evaporation, precipitated with diethyl ether and collected by gravity filtration. The monosubstituted product was purified by silica column chromatography using a solvent mixture of methanol (MeOH): DCM (3L; 1:9 vol.). The purified monosubstituted product was concentrated by rotary evaporation and dried using a lyophilizer. Yield: 1.91g (32%). The monosubstituted heterobifunctional carboxy PEG was generated by deprotection of the monosubstitued product by stirring in 15mL solution of 3:7 (v/v) trifluroacetic acid (TFA) to DCM at RT for 24 h The resulting solution was concentrated by rotary evaporation and redissolved in 15mL of DCM to which was added 150mg Amberlyst A21. The solution was stirred for further 24h at RT. The product was obtained by rotary evaporation and lyophilized for 18h The PEGC polymer silane was synthesized by dissolving the heterobifunctional polymer in 15mL of DCM to which was added triethoxysilylpropyl isocynate (TESPI) at 1:1.1 molar ratio. The resulting solution was stirred in an ice bath for 48h. The product was concentrated by rotary evaporation and dried by lyophilization.

1. 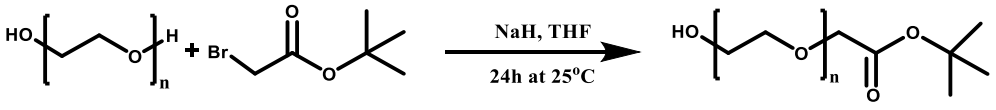

2. 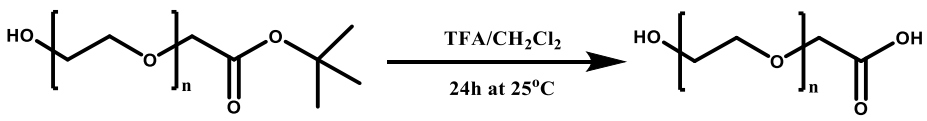

3. 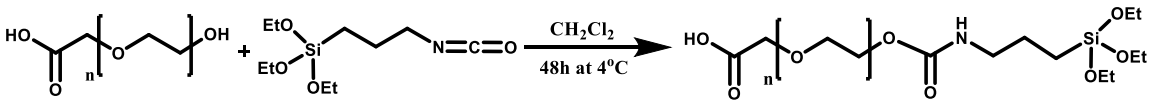

Scheme 1. Three-step procedure for the synthesis of poly (ethylene) glycol (PEGC) linker.

2.3 Synthesis of PEGylated Mesoporous Silica Nanoparticles

Grafting of the as-synthesized PEGC polymers to FITC-labeled MSNs was carried out by ethanolic reflux of MSNs and polymers. Grafting of PEGC was carried out using 50mg of FITC-MSNs and 25mg of PEGC with 40 µL of NH_4OH (35% v/v) in 50mL of ethanol and refluxing at 90^oC for 18h with constant stirring. The PEG-grafted MSNs were collected by centrifugation, washed 3x with EtOH and resuspended in EtOH. The extent of PEGC polymer grafting on all materials was determined by TGA.

2.4 Covalent Modification of Mesoporous Silica Nanoparticles with Cholera Toxin Subunit B

Covalent attachment of CTxB was conducted using EDC-mediated carbamide coupling of the acid functional groups on the surface of PEGC-MSNs to free amines of CTxB (Scheme 2). The covalent attachment of CTxB was carried out by dispersing 10mg of PEGC-MSN in 10mL of DI water to which was added 0.74 µg of EDC with 250µg of CTxB. The resulting solution was stirred for 48h at 4^oC under dark conditions. The CTxB-modified MSNs were obtained by centrifugation, washed 3x with DI water and resuspended in DI water. The extent of CTxB attachment was determined by Pierce^{TM} BCA protein quantification assay on the reaction supernatant using an enhanced protocol.

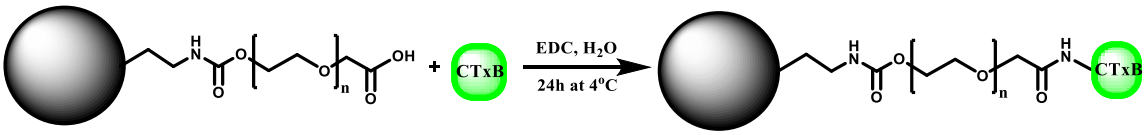

Scheme 2. EDC-mediated carbamide coupling for covalent attachment of CTxB to MSN materials.

2.5 Culture of Human Cervical Carcinoma (HeLa) Cell Line

HeLa cells were maintained in a 37°C, 5% carbon dioxide environment in RPMI 1640 medium supplemented with 10% (v/v) fetal bovine serum and 2% (v/v) penicillin/streptomycin. For endocytosis and receptor inhibition assays, cells were seeded at $2x10^5$ cells/well in 6-well tissue culture plates and incubated for 36h. For fixed-cell confocal imaging, cells were seeded at $2x10^5$ cells/well in 8-well chambered coverglass and incubated for 24h. For all cytotoxicity assays, cells were seeded at $1x10^5$ cells/ml in 96-well microtiter culture plates and incubated for 24h. The concentrations of the materials used for all experiments in this work were selected according to the minimum concentration that resulted in no less than 90% total cell viability at the aforementioned cell count (Figure A1).

2.6 Intracellular Uptake and Endocytosis Inhibition Assays

The cell medium was aspirated and the cultured cells were treated with Wortmannin (240nM, 30min) to inhibit macropinocytosis, Chloropromazine (10.66µg/ml, 30min) to inhibit clathrin-mediated endocytosis, and Genistein (50µg/ml, 30min), and nystatin (25µg/ml, 30min) to inhibit caveolae-mediated endocytosis respectively. For the simultaneous inhibition of MPC and CME or MPC, CME, and CAVME, cells were incubated with Wortmannin/Chloropromazine or Wortmannin/Chloropromazine/Genistein in minimal medium using the aforementioned

concentrations. The medium was aspirated and to each well was added 50μg of MSN, PEGC-MSN, or CTxB-MSNs suspended in RPMI 1640 minimal medium. The cells were incubated with each material for 1h, after which the medium was aspirated and replace with RPMI 1640 medium supplemented with FBS. All cells were incubated a further 2h prior to being harvested with trypsin and fixed (4% (v/v) Paraformaldehyde in PBS). The cells were resuspended in 300μL of PBS and transferred to 5mL polystyrene round bottom tubes to which was added 100μL trypan blue solution. To each cell suspension was added 20μL of a10μg/mL propidium iodide staining solution to identify dead cells to be excluded from the analysis. The cellular fluorescence resulting from internalization of each material was quantified using FACS. Prior to harvesting, all cells were washed 2x with PBS between each treatment.

2.7 Cholera Toxin Subunit B Receptor Specificity Assays

Cells were cultured for 4.5 days in medium containing 5μM 1-phenyl-2-hexa-decanoylamino-3-morpholino-1-propanol (PPMP). The cells were harvested and reseeded in 6-well tissue culture plates at the indicated concentration and incubated for an additional 36h using the same conditions. The medium was aspirated and to each well was added 50μg of MSN, PEGC-MSN, or CTxB-MSN suspended in RPMI 1640 minimal medium. The cells were incubated with each material for 1h, after which the medium was aspirated and replace with RPMI 1640 medium supplemented with FBS and incubated an additional 2h. The cells were then prepared for FACS using the aforementioned procedure and the levels of internalization for each material quantified. For competitive binding inhibition using free CTxB, cells were seeded in 6-well tissue culture plates at the indicated concentration and incubated for 36h using the same

conditions. The medium was aspirated and to each well was added a solution containing ≈10x amount of CTxB as was present on 50μg of CTxB-MSN in RPMI 1640 minimal medium. The cells were incubated for 30min at 37°C, afterwards the medium was aspirated and replaced with 50μg of MSN, PEGC-MSN, or CTxB-MSN suspended in RPMI 1640 minimal medium. The cells were incubated with each material for 1h, after which the medium was aspirated and replace with RPMI 1640 medium supplemented with FBS and incubated an additional 2h. The cells were then prepared for FACS using the aforementioned procedure and the levels of internalization for each material quantified.

2.8 Fixed-Cell Laser Scanning Confocal Microscopic Imaging of Silica Nanoparticle Intracellular Dynamics

2.8.1 Lysosomal Colocalization

The cell medium was aspirated and replaced with serum-free medium containing 25 μg/mL of MSN, PEGC-MSN, or CTxB-MSN. After 30 min the medium was aspirated and cells were stained with Lysotracker Red DND-99 (500nM) to selectively label lysosomes. After incubating for 30min the staining solution was aspirated, the cells washed with PBS, and fixed with a 4% (v/v) paraformaldehyde solution. After fixing for ≈1h, the fixing solution was aspirated, the cells washed with PBS, and counterstained with nuclei-staining dye Hoescht 33342 (5μg/mL). The cells were incubated for 30min before the staining solution was aspirated and the cells washed with PBS. The same solution was then added to each well and the intracellular localization of all materials determined by laser scanning confocal microscopy.

2.8.2 Endoplasmic Reticulum Colocalization

The cell medium was aspirated and replaced with serum-free medium containing 25 μg/mL of MSN, PEGC-MSN, or CTxB-MSN. After 30 min the medium was aspirated and cells were stained with ERtracker Blue-White DPX (5μM) to selectively label the endoplasmic reticulum. After incubating for 30min the staining solution was aspirated, the cells washed with PBS, and fixed with a 4% (v/v) paraformaldehyde solution. After fixing for ≈1h, the fixing solution was aspirated and the cells washed with PBS. The same solution was then added to each well and the intracellular localization of all materials determined by laser scanning confocal microscopy.

2.8.3 Golgi Apparatus Colocalization

The cell medium was aspirated and replaced with serum-free medium containing 25 μg/mL of MSN, PEGC-MSN, or CTxB-MSN. After 30 min the medium was aspirated and cells were stained with BODIPY-TR Ceramide (25μM) to selectively label the golgi apparatus. After incubating for 30min the staining solution was aspirated, the cells washed with PBS, and fixed with a 4% (v/v) paraformaldehyde solution. After fixing for ≈1h, the fixing solution was aspirated, the cells washed with PBS, and counterstained with nuclei-staining dye Hoescht 33342 (5μg/mL). The cells were incubated for 30min before the staining solution was aspirated and the cells washed with PBS. The same solution was then added to each well and the intracellular localization of all materials determined by laser scanning confocal microscopy.

2.8.4 Endoplasmic Reticulum/Lysosomal Colocalization

For the double-staining experiments, the cell medium was aspirated and the cells treated with Lysotracker for 30 min. After removal of the cell medium, the cells were

then inoculated with a 25μg/mL suspension of MSNs, PEGC-MSNs, or CTxB-MSNs in serum-free cell medium. After 30 min, the medium was aspirated and the cells were stained with ERtracker for additional 30 min. Finally, the staining solution was removed and the cells fixed with a 4% (v/v) paraformaldehyde solution. After fixing for ≈1h, the fixing solution was aspirated and the cells washed with PBS. PBS was then added to each well and the intracellular localization of all materials determined by laser scanning confocal microscopy.

2.8.5 Colocalization analysis

Quantitative colocalization analysis was performed using a method similar to that used by Pollock et al.[26] Briefly, a region of interest (ROI) was defined for each cell encompassing all labeled cellular structures. Noise was removed from the defined ROI using a median filter set to 3x3 pixels, and Manders correlation coefficients calculated using thresholds set at the mean + 1 SD intensity for each image channel. The colocalization of each material for all single label experiments was reported as the frequency of localization in each of the different cellular organelles investigated in this work (two groups of 5 cells per condition). For the double labeling experiments colocalization was reported as total mean colocalization. All analysis was done through ImageJ using the JaCoP plug-in.[27]

2.9 Propidium Iodide Loading and Intracellular Delivery

Propidium iodide was loaded in each material using the following procedure: 25μg of MSN, PEGC-MSN, and CTxB-MSN was resuspended in a 250μg/mL solution of PI in DI H_2O and stirred under dark conditions for 18h. The materials were collected by centrifugation and resuspended in 1mL of serum-free media prior to inoculation. The cell

culture medium was aspirated and replaced with the serum-free medium containing 25 μg/mL of PI-loaded MSN, PEGC-MSN, or CTxB-MSN. After 1h, the medium was aspirated, the cells washed with PBS, supplemented culture medium added to each well, and the cells incubated another 24h. The medium was then removed, the cells washed with PBS, and stained with ERtracker Blue-White DPX (5μM) to selectively label the endoplasmic reticulum. After incubating for 30min the staining solution was aspirated, the cells washed with PBS, and fixed with a 4% (v/v) paraformaldehyde solution. After fixing for ≈1h, the fixing solution was aspirated and the cells washed with PBS. The same solution was then added to each well and the cells imaged by laser scanning confocal microscopy.

2.10 Statistical Analysis

All statistical analyses were performed using Microsoft Excel software. All graphs represent means ± SD of all values. All *P* values for intracellular uptake were determined using two-tailed Student *t* tests. The *P* values for comparisons of material subcellular localization were made using one-tailed Student *t* tests.

CHAPTER 3: RESULTS AND DISCUSSION

3.1 Synthesis of MSN Materials

3.1.1 Synthesis of Mesoporous Silica Materials

The synthesis of fluorescein-labeled MSNs was carried out by using a surfactant-templated co-condensation approach that was modified from the literature.[24] The surfactant was removed by an acid wash in methanolic solution under reflux. The complete structural properties of the MSN material were analyzed by N_2 sorption isotherms (BET method), dynamic light scattering (DLS), ζ-potential, transmission electron microscopy (TEM), and thermogravimetric analysis (TGA). The BET analysis of the N_2 sorption isotherms (Figure 4) shows that the MSN material has a surface area of 377.6 m^2/g. The hydrodynamic diameter of this material was found to be 450.2 nm in simulated physiological environment (PBS, pH 7.4, 10mM) and 152.5 nm in water. The surface of the MSNs is negatively charged due to the presence of deprotonated silanols on the surface of the nanoparticles as evidenced by the ζ–potential (-16.2 ± 0.45 mV) (Table 1). TEM micrographs showed the MSNs to be monodisperse, with spherical morphologies and diameters of 35.8 ± 5.8 nm (Figure 6). The amount of fluorescein dye chemically attached to the interior channels of the FMSNs was found by TGA to be approximately 8.1 wt.%, by weight (Figure 5). Carboxylic acid-PEG(PEGC)-silane polymers were grafted to the MSNs to afford the corresponding PEGC-MSN material. The BET analysis of PEGylated MSN materials shows a reduction in the surface area due

to the presence of the PEG molecules blocking the entrance of the MSN pores (Table 1). The PEGC-MSN material exhibits poor colloidal stability in PBS and improved stability in water with hydrodynamic diameters of 139.7nm. The decrease in the ζ–potential value (-18.0 ± 0.31 mV) for the PEGC-MSNs verify the presence of the PEGC polymer molecules on the MSN material. TGA confirmed the presence of PEG moieties on the surface of MSNs with the organic content of PEGC-MSNs increasing by 4.1% in comparison with MSNs. The PEGC-MSN particles were further functionalized with CTxB protein to afford CTxB-MSN materials. The CTxB protein was covalently attached to PEGC-MSNs by an EDC-mediated carbamide coupling reaction. The amount of CTxB attached to PEGC-MSNs was quantified by determining the amount of residual protein in the supernatant using a calorimetric BCA protein quantification assay. Using this approach, the amount of CTxB protein chemically attached to PEGC-MSNs was found to be 7.1±1.3μg CTxB/mg of material.

Table 1. Structural characterization data for MSN materials.

Material	Hydrodynamic diameter H_2O (nm)/PdI	Hydrodynamic diameter in PBS (nm)/PdI	ζ-potential (mV)	Organic content (%)	Surface Area (m^2/g)
MSN	152.5/0.306	450.2/0.446	-16.2 ± 0.4	8.1	377.6
PEGC-MSN	139.7/0.097	1442/0.978	-18.0 ± 0.3	12.2	314.1
CTxB-MSN	164.30/0.223	759.8/0.399	-19.3 ± 1.1	---	---

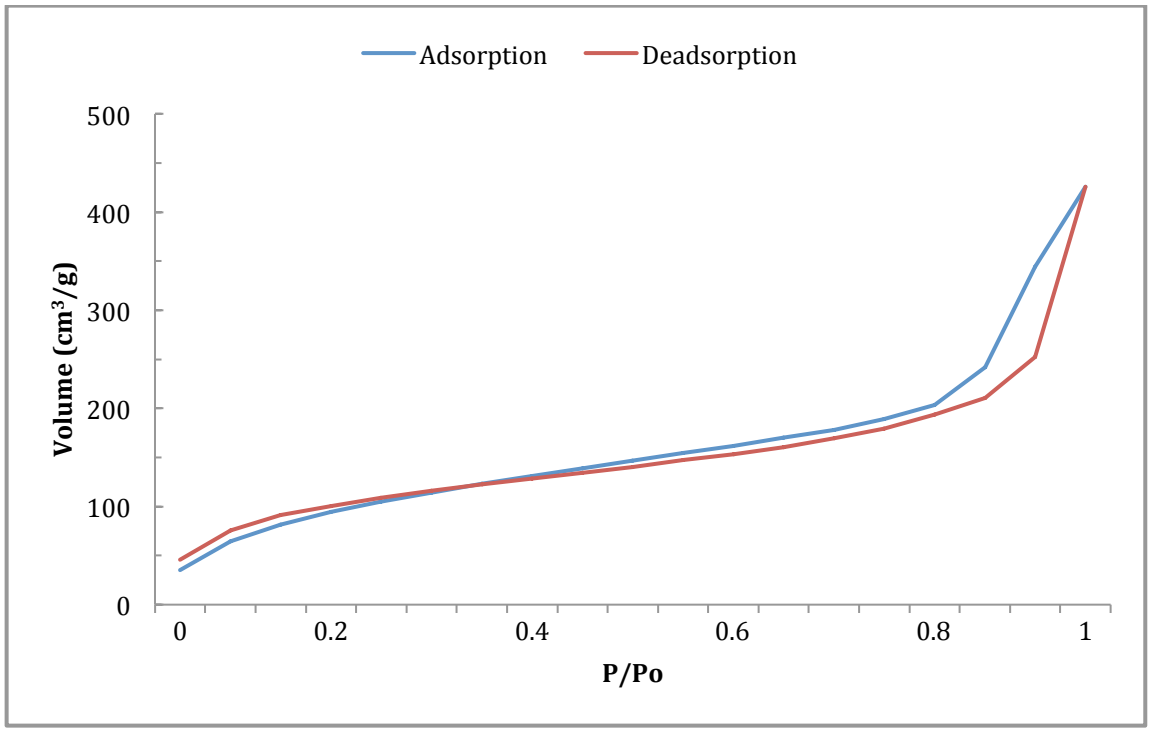

Figure 4. Nitrogen absorption/desorption isotherms for MSN material.

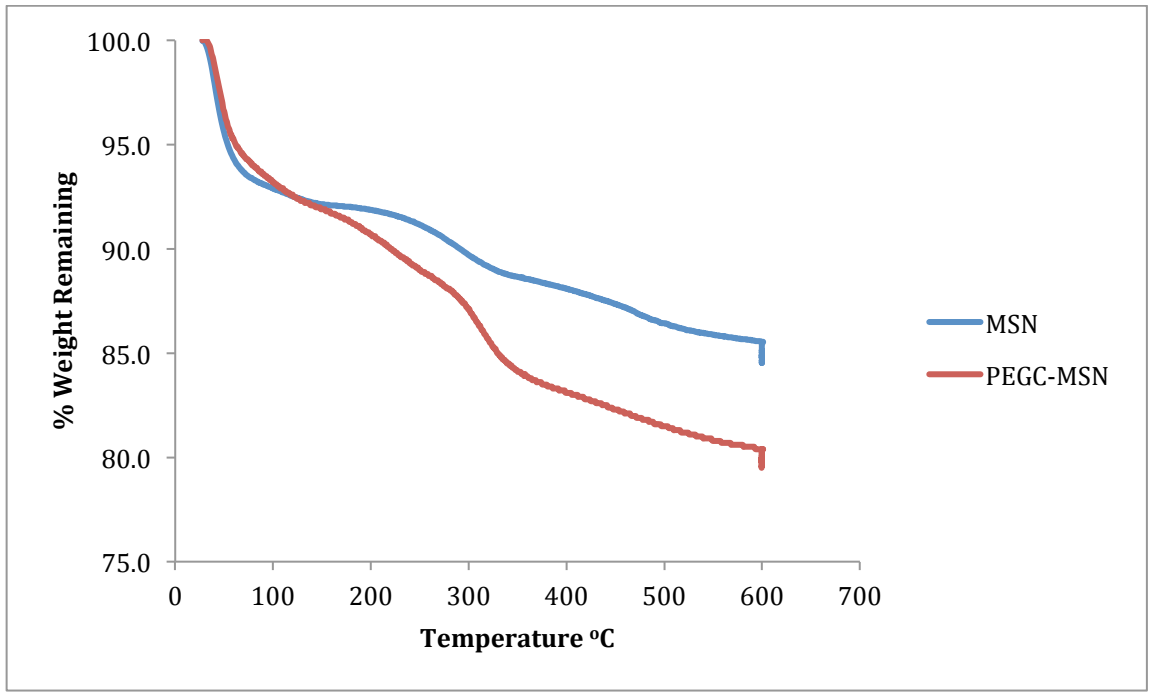

Figure 5. Thermogravimetric analysis of MSN and PEGC-MSN materials.

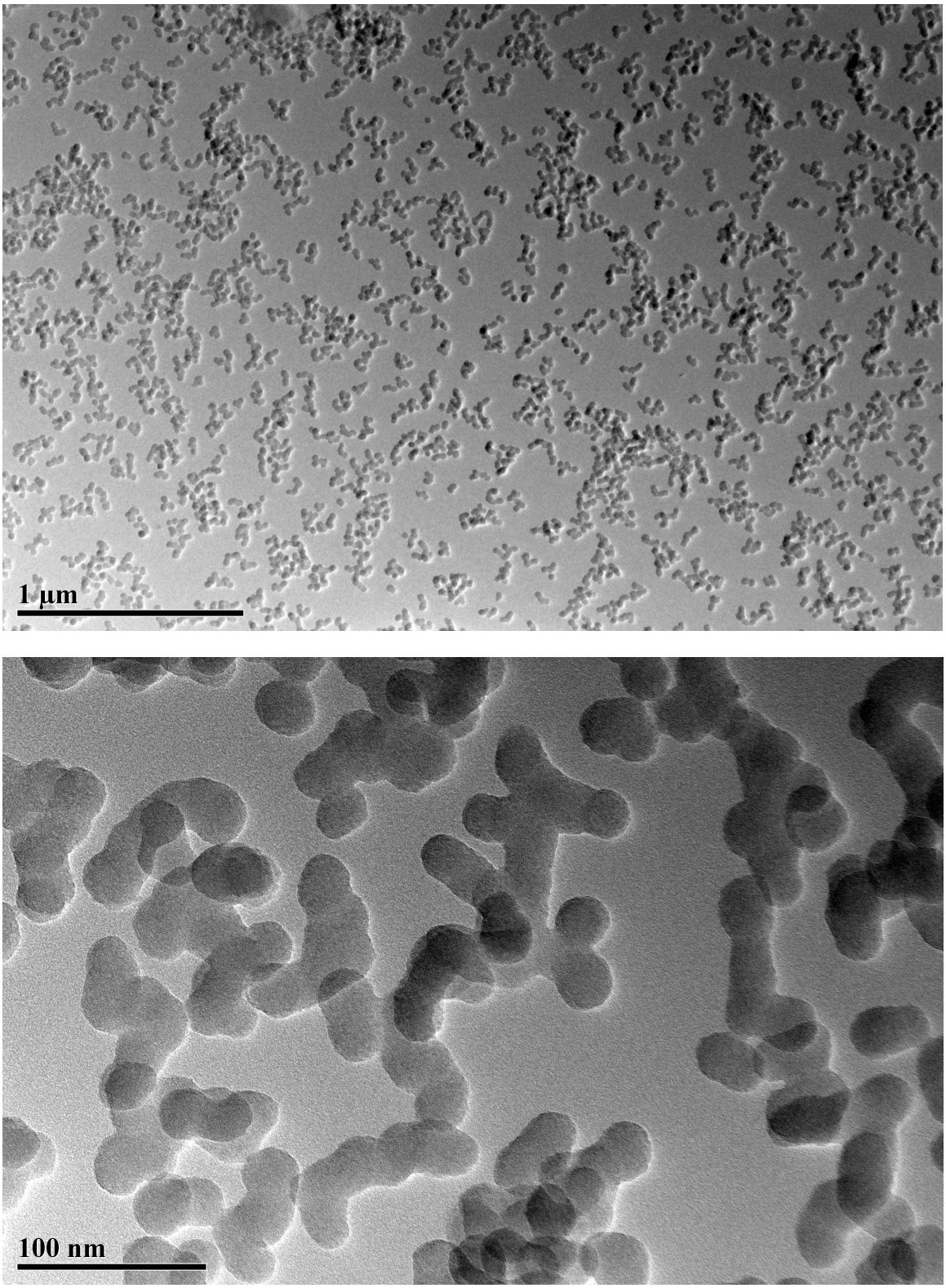

Figure 6. TEM micrographs of MSN materials show synthesized materials exhibit uniform size (top) and structure (bottom).

3.2 Determination of MSN Cellular Uptake Pathways

Inhibition of select endocytic pathways was used to determine the means of internalization utilized by cells for the uptake of each material. Chemical inhibitors known to suppress cellular endocytosis and their effective concentrations were selected according to the literature[9]. Wortmannin was used to evaluate the role that macropinocytosis, a common macroscale endocytic pathway, played in the uptake of MSN materials. This agent irreversibly binds to the catalytic subunit of phosphatidylinositol-3 (PI-3) kinase, which regulates the arrangements of actin filaments.[28] The presence of Wortmannin resulted in an increase in the uptake of MSN (117.7 ± 5.2% (P=0.02)) but did not significantly affect the internalization of PEGC-MSNs (106.5 ± 7.8% (P=0.34)) or CTxB-MSN materials (98.7 ± 5.9% (P=0.69)) (Figure 7). The effect of clathrin inhibition on MSN particle uptake was tested by using the cationic amphiphilic drug chlorpromazine, which causes dissociation of clathrin from the plasma membrane, inhibiting the formation of clathrin-coated pits.[29,30] The uptake of MSN (66.3 ± 0.45%(P=0.002)) in chlorpromazine-treated cells was significantly reduced in agreement with previous reports that have shown these materials to be internalized by clathrin-mediated endocytosis.[31] Interestingly, the uptake of PEGC-MSN (127.3 ± 3.8% (P=0.02)) and CTxB-MSNs (115.0 ± 5.8% (P=0.04)) is increased in the presence of chlorpromazine (Figure 7). To examine whether caveolae-mediated endocytosis, a well-studied non-clathrin route of cellular entry, played a role in the endocytosis of MSN materials, the uptake of particles in the presence of caveolae-inhibiting agents, genistein and nystatin was investigated. Genistein, a tyrosine kinase inhibitor, has been shown to inhibit the caveolae-mediated endocytosis by destabilizing actin and preventing the

recruitment of dynamin to the site of endocytosis.[32] Nystatin binds cholesterol in the plasma membrane, disrupting lipid-rafts and impeding the formation of caveolae-coated vesicles.[33] Inhibition of caveolae-mediated endocytosis with genistein and nystatin increased the uptake of MSNs (150.1 ± 17.5%(P=0.05) and 157.6 ± 9.6%(P=0.01), respectively). The uptake of PEGC-MSN particles exhibited a less dramatic increase in cells treated with genistein (109.9 ± 2.7(P=0.03)) and nystatin (123.1 ± 2.6(P=0.001)), suggesting that caveolae-mediated mechanisms are not involve in their uptake or trafficking. As expected, genistein and nystatin did reduce the uptake of CTxB-MSNs (79.9 ± 3.3%(P=0.009) and 80.0 ± 3.3%(P=0.04), respectively) (Figure 7). Simultaneous inhibition of two and three internalization pathways was also investigated to uncover possible synergy between pathways in the uptake of the materials. Double inhibition in the presence of Wortmannin (macropinocytosis) and chlorpromazine (clathrin-mediated endocytosis) reduced the internalization of MSN (59.1 ± 6.9%(P=0.004)) with no significant change in the uptake PEGC-MSNs (124.6 ± 9.6% (P=0.06)), and CTxB-MSNs (147.8 ± 18.9%(P=0.06)). Further inhibition of caveolae-mediated endocytosis did not change the reduction in uptake of MSNs (61.5 ± 1.6%(P=0.001)) although an increase in the uptake of PEGC-MSNs (123.7 ± 4.4%(P=0.03)) and CTxB-MSNs (128.1 ± 8.6% (P=0.04)) was observed.

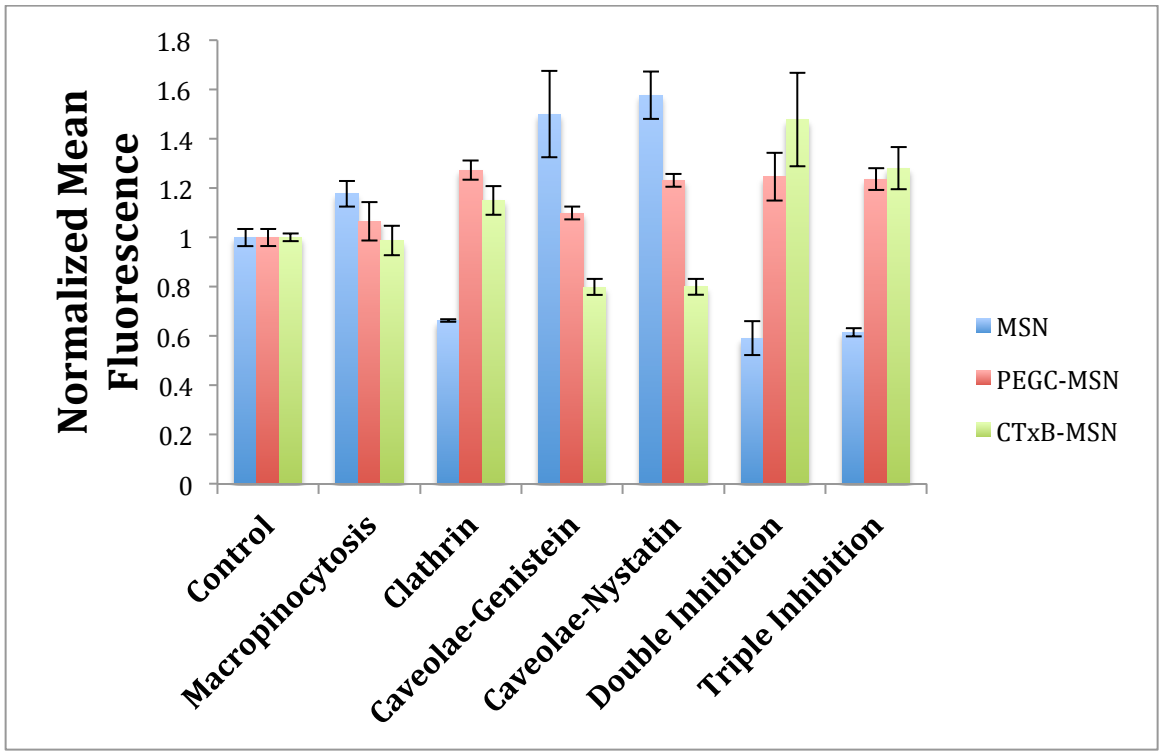

Figure 7. Endocytosis inhibition assays for MSN materials. Uptake of material for all conditions normalized to corresponding untreated control.

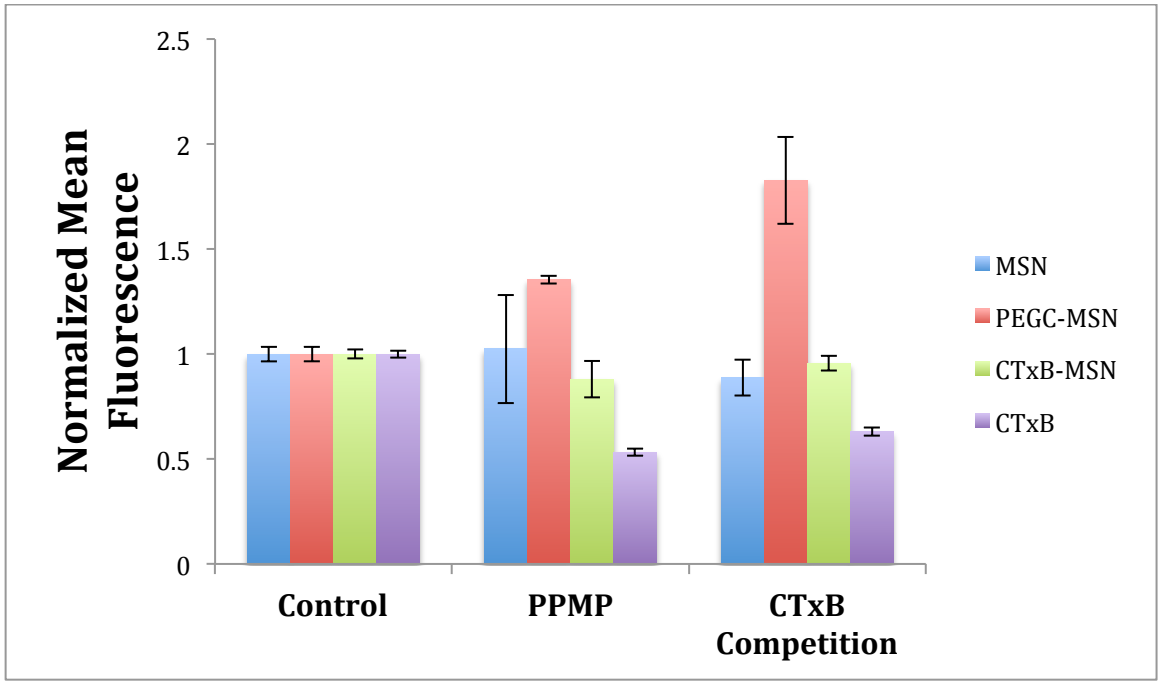

Figure 8. GM_1 receptor uptake inhibition assay. Uptake of material for all conditions normalized to corresponding untreated control.

3.3 GM_1 Receptor Specificity of CTxB-modified MSNs

The internalization of the native cholera holotoxin is initiated by binding of the B subunit to the cell surface ganglioside GM_1.[34] To better understand the influence of bound CTxB on the uptake of MSNs, GM_1 was chemically inhibited. The ceramide analogue 1-phenyl-2-hexa-decanoylamino-3-morpholino-1-propanol (PPMP) is a known inhibitor of ganglioside synthesis[35] and has been used extensively to study the uptake of both cholera and shiga toxin.[36] Inhibition of ganglioside synthesis using the ceramide analogue PPMP significantly inhibited the uptake of free FITC-labeled CTxB (53.3 ± 1.7%($P<0.0001$)) (Figure 8), indicating that PPMP was effectively inhibiting synthesis of the Cholera toxin binding ligand GM_1. No change was observed in the uptake of MSNs (102.4 ± 25% ($P=0.88$)) as would be expected of their nonspecific uptake. Conversely, PEGC-MSN internalization (135.4 ± 1.9% ($P=0.001$)) was significantly elevated above its respective control. Inhibition of GM_1 synthesis with PPMP did not however cause a significant decrease in the uptake of CTxB-MSNs (87.9 ± 8.6% ($P=0.12$)). A similar outcomes were observed when the GM_1 receptor was blocked with an excess of free, unlabeled CTxB. Control experiments with FITC-labeled CTxB protein demonstrate that the GM_1 receptors in HeLa cells could be blocked in the presence of CTxB protein (63.1 ± 1.9% ($P=0.001$)). A small change in the internalization of MSNs (88.6 ± 8.5% ($P=0.001$)) was observed along with a significant increase in the uptake of PEGC-MSNs (182.8 ± 20.7%($P=0.02$)). For CTxB-MSNs, no significant change in uptake in the presence of free CTxB could be observed (95.6 ± 3.5% ($P=0.14$)), making it difficult to determine whether or not GM_1 plays a role in the uptake of these materials.

3.4 Intracellular Localization of MSN Materials

3.4.1 Lysosomal Colocalization

Like many other nanomaterials, MSNs are often detained in degradative lysosomes following uptake. Laser scanning confocal microscopy of HeLa cells stained with Lysotracker Red (DND-99), a fluorescent probe that selectively accumulates in acidic organelles, was used to investigate the intracellular localization of these materials. Fluorescin-labled MSNs were shown to colocalize exclusively with lysosomes (95.0 ±7% frequency of colocalization) in agreement with previous reports.[17] PEGC-MSNs were also shown to colocalize extensively with cellular lysosomes following internalization (75.3 ± 8%). Conversely, a significantly lower percentage of CTxB-MSNs were found to colocalize with lysosomes (51.1 ± 1.6% (P=0.04)), suggesting that these materials are better able to evade lysosomal entrapment (Figure 9, Figure 10, and Figure B1).

3.4.2 Golgi Apparatus Colocalization

The intracellular behavior of CTxB causes it pass transiently through the golgi apparatus (GA) prior to arriving in the ER. To determine if CTxB-MSNs localize with this cellular organelle, the GA was selectively stained (BODIPY-Ceramide TR conjugated to BSA™) and colocalization of all materials with this structure evaluated (Figure 10 and Figure B2). From this, it could be concluded that MSN and PEGC-MSN do not colocalize with the GA (17 ± 9.9% and 10±14.1% respectively). Meanwhile, the frequency of colocalization of CTxB-MSNs with the GA (40 ± 0% (P=0.03)) was higher than that observed for the other materials, suggesting that CTxB-MSN conjugates transiently exist within the GA following uptake (Figure 9).

3.4.3 Endoplasmic Reticulum Colocalization

Cholera Toxin is known to traffic to the Endoplasmic reticulum following uptake by its target cells. To determine if CTxB-conjugated MSNs are capable of localizing to the ER, colocalization of fluorescein-labeled MSN materials with the ER (labeled with ER-Tracker™ Blue-White DPX) was evaluated (Figure 10 and Figure B3). From this it was determined that MSNs and PEGC-MSNs do not exhibit consistent levels of colocalization with the ER (40 ± 28.3% and 44.7 ± 2.8% respectively) (Figure 9). Conversely, CTxB-MSNs were found to localize more frequently with the ER (60 ± 28.3%) although this difference in colocalization between materials was not found to be significant.

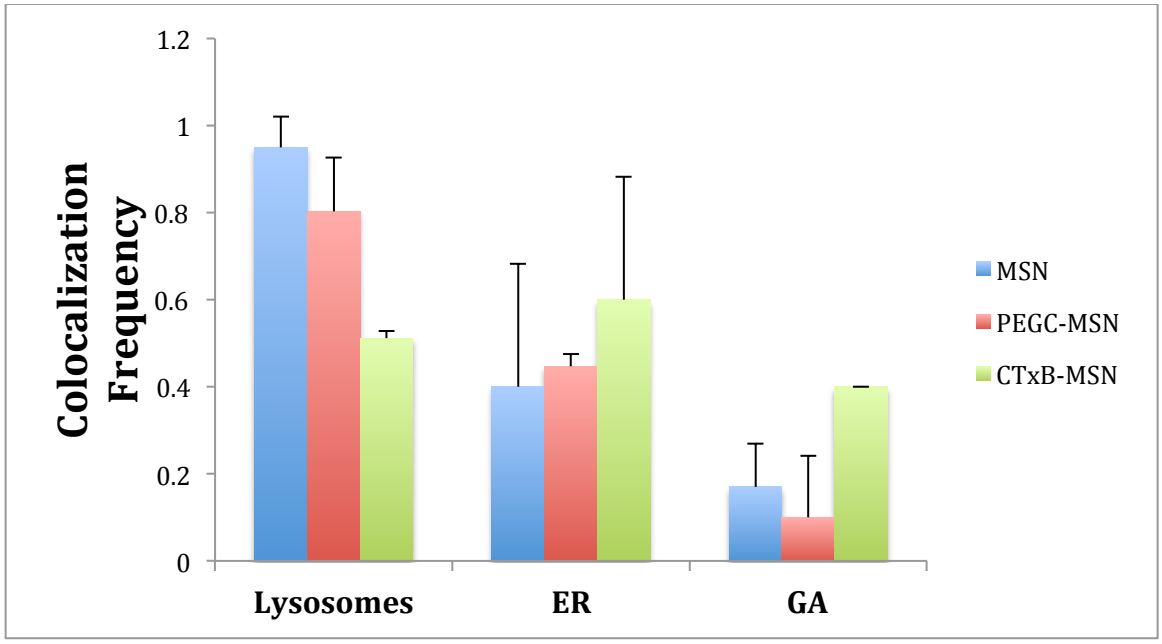

Figure 9. Frequency of colocalization of each material with lysosomes, GA, and ER as determined by LSCM.

3.4.4 Relative Colocalization in Endoplasmic Reticulum and Lysosomes

To determine whether MSNs colocalize predominantly with lysosomes or the ER, these organelles were simultaneously labeled and the resultant colocalization of MSNs with these structures evaluated (Figure 11 and Figure B4). In support of previous

observations, MSNs and PEGC-MSNs were found to colocalize extensively with lysosomes (75.2 % and 71.5 % mean colocalization respectively) even in instances where they appeared to overlap with the ER (40.9% and 54.5 % mean colocalization respectively), indicating that these materials were contained within the lysosomes and not the ER.

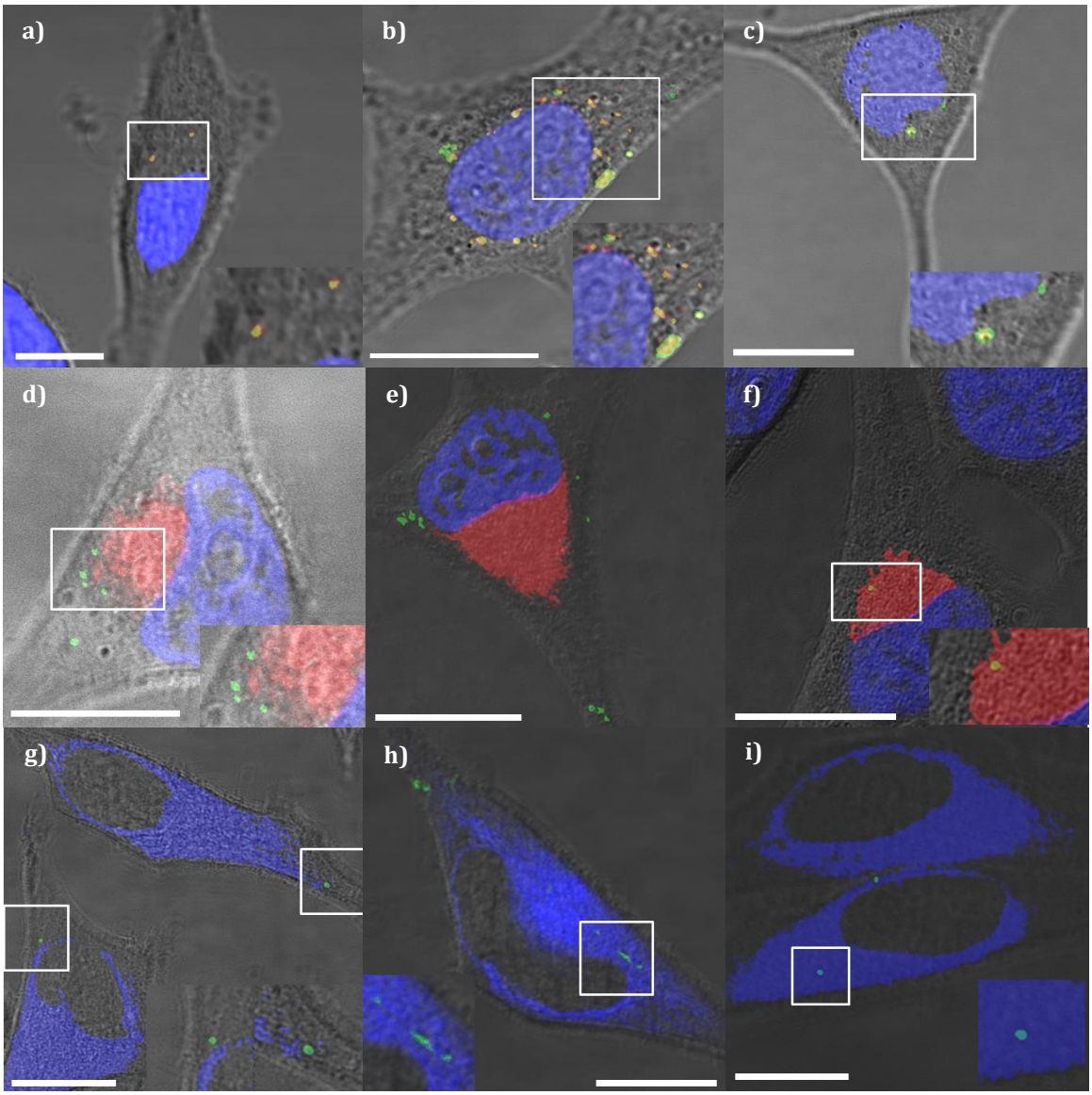

Figure 10. Representative images for MSN (a,d,g), PEGC-MSN (b,e,h), and CTxB-MSN (c, f, i) for lysosomal (top), golgi apparatus (middle), and endoplasmic reticulum (bottom) colocalization. All the scale bars are 10 μm in size.

3.5 Demonstration of *In vitro* Small Molecule Delivery by CTxB-MSNs

The ability of CTxB-MSNs to traffic through the cell in a retrograde fashion would enable this material to more efficiently deliver sensitive therapeutic molecules to their respective organelle targets such as the cytoplasm, ER and nucleus. As proof of this concept, propidium iodide (PI) was physically loaded into CTxB-MSNs (PI-loaded CTxB-MSNs) to demonstrate that CTxB-MSNs can deliver and release this molecule.

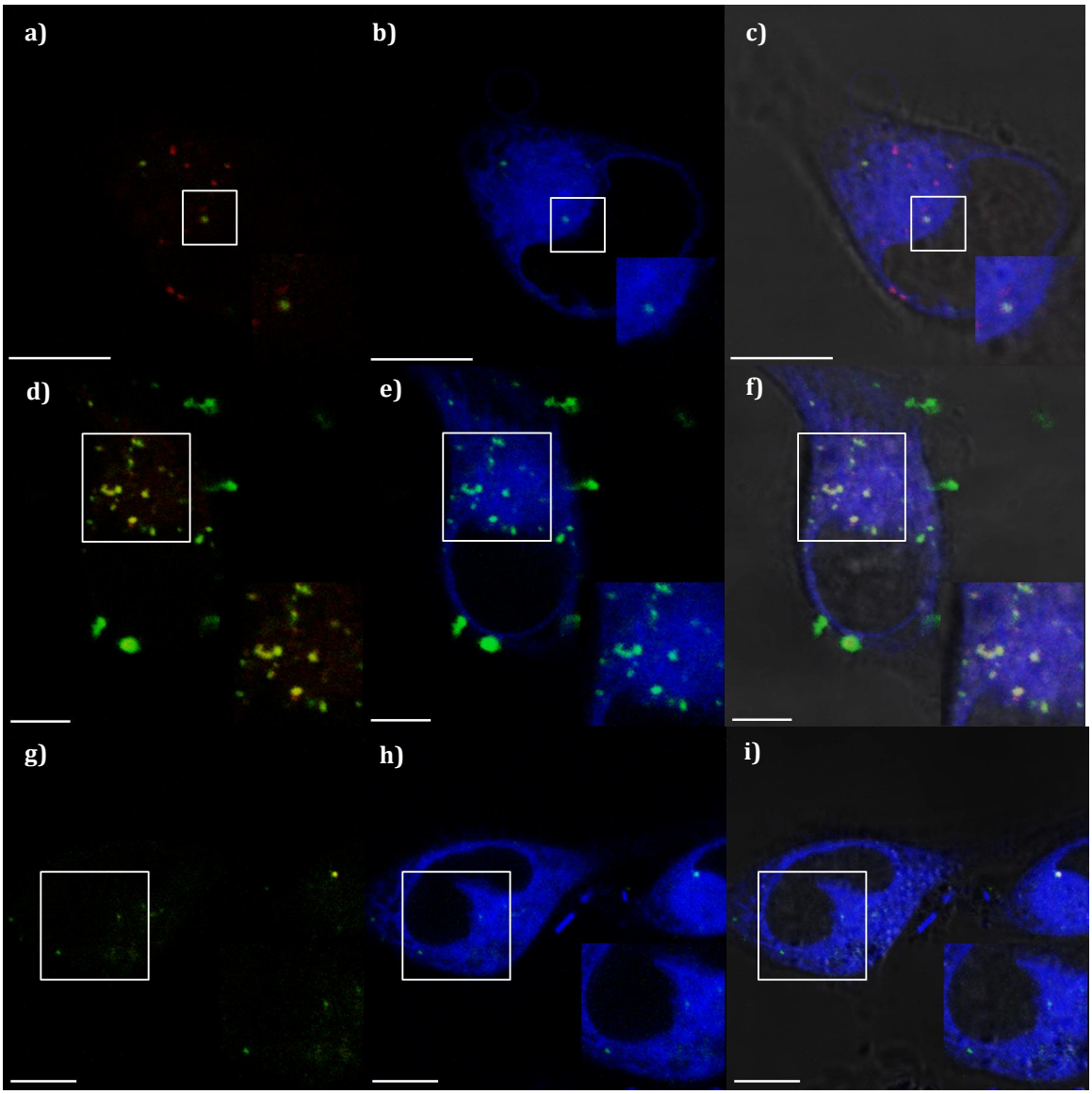

Figure 11. Representative confocal images for MSN (a,b,c), PEGC-MSN (d,e,f), and CTxB-MSN (g, h, i) for lysosomal and endoplasmic reticulum colocalization.
All the scale bars are 10 μm in size.

PI is a fluorescent DNA intercalating agent, is impermeable to the cell membrane, and is excluded from viable cells. PI is commonly used for identifying dead cells in a population and as a counterstain in multicolor fluorescent techniques.[37] HeLa cells were inoculated with PI-loaded MSN materials (MSNs, PEGC-MSNs and CTxB-MSNs) for 1h and incubated for another 23h prior to fixation. To investigate whether the MSN particles were colocalized with the ER, the cells were stained with ER-Tracker™ Blue-White DPX. LSCM images show that PI-loaded CTxB-MSNs are internalized by HeLa cells (Figure 12a) and that the PI dye has been efficiently released inside the cell (Figure 12b). ER staining shows the diffusion of PI molecules colocalized with the ER (Figure 12c), indicating that the membrane impermeable dye has been trapped in this organelle. Interestingly, some of the PI molecules have diffused to the cell nucleus and localized in what appears to be the nucleolus (Figure 12d). This supports the hypothesis that CTxB-MSNs can transport PI molecules inside HeLa cells through the retrograde pathway and release them in the ER and, consequently, to the nucleus. In the case of PI-loaded MSNs and PEGC-MSNs, LSCM images show that both are internalized by HeLa cells. However, the intracellular release of the PI molecules from MSN (Figure B5) and PEGC-MSN materials was not observed (Figure B5). The absence of diffusion of the fluorophore from the material carrier indicates that these materials are still trapped in the lysosomes, preventing the diffusion of PI molecules away from the MSN particles.

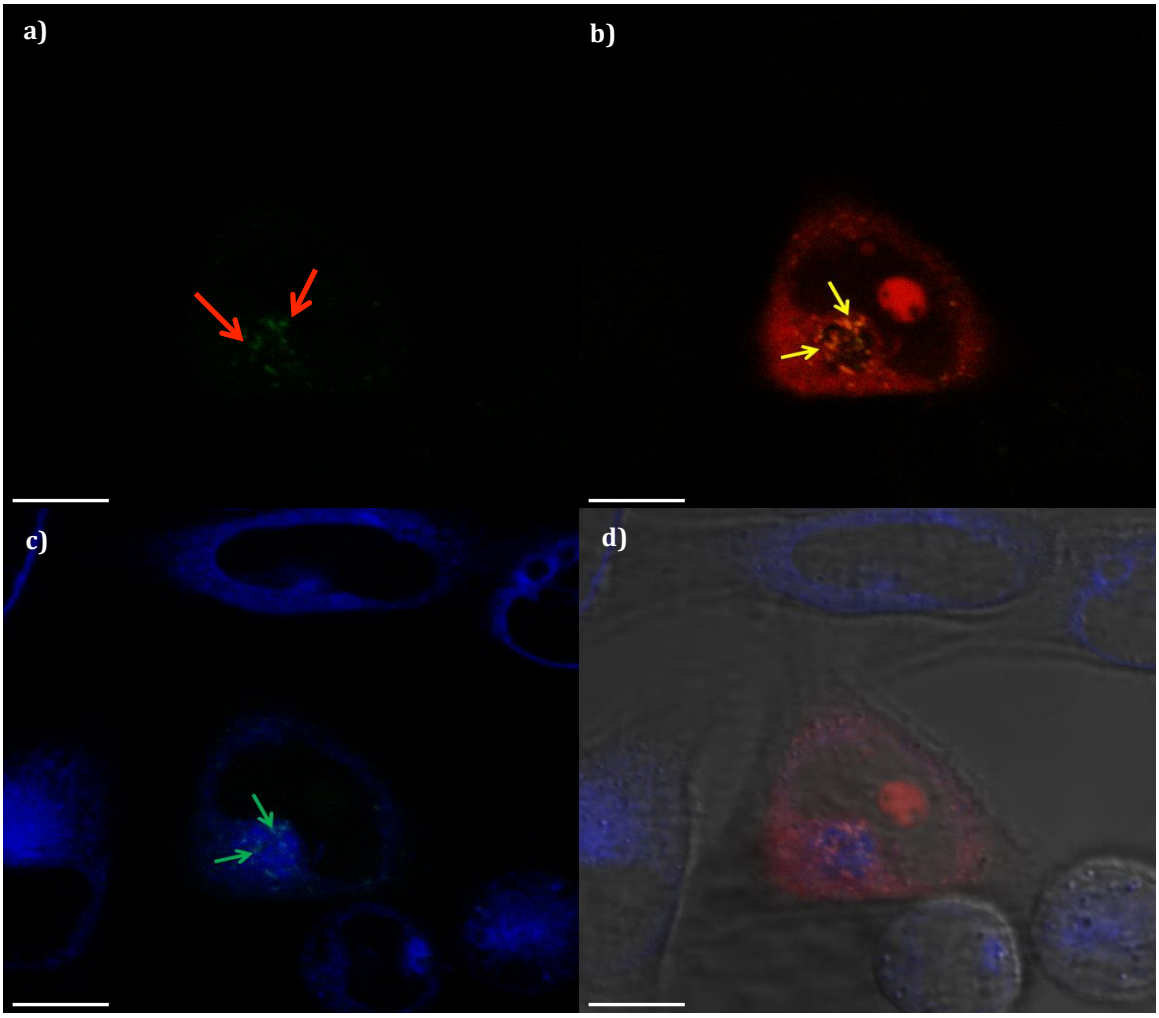

Figure 12. LSCM images detailing the intracellular delivery of PI mediated by CTxB-MSNs in HeLa cells. LSCM images of HeLa cells inoculated with PI-loaded CTxB-FMSNs. a) CTxB-MSNs (green). b) CTxB-MSN overlap with PI molecules (red). c) ER-stained image super-imposed over CTxB-MSNs. d) Merge of the previous images with the DIC channel. All the scale bars are 10 μm in size.

CHAPTER 4: CONCLUSIONS AND FUTURE WORK

Previous investigations into the intracellular behavior of nanoscale materials have revealed that they exhibit near uniform subcellular localization in lysosomes, the degradative organelles of the cell. This presents a serious challenge for the delivery of therapeutic molecules, as containment in the lysosome will limit therapeutic outcomes by degrading and/or preventing them from reaching their cellular targets. Herein, we have attempted to influence the intracellular localization of mesoporous silica nanoparticles by modifying their surface with a protein known to exhibit alternate intracellular trafficking and subcellular localization. The B subunit of the bacterially-derived protein, cholera toxin, belongs to a group of proteins known to traffic in a retrograde fashion following internalization by their target cells. Upon interacting with their respective cellular receptors at the plasma membrane, these proteins move via endosomes through the trans-golgi network to the endoplasmic reticulum. By covalently modifying the surface of MSNs with CTxB, we aimed to emulate the retrograde trafficking behavior of the native protein and improve intracellular delivery by avoiding lysosomal entrapment. In this work, mesoporous silica nanoparticles modified with the CTxB proteins were successfully synthesized using conventional bioconjugation methods and their subsequent cellular interactions determined *in vitro*. The uptake of CTxB-modified MSNs was found to be partially dependent of caveolae-mediated endocytosis and insensitive to inhibitors for other endocytic pathways in accordance with what has been previously reported for

the native protein.[38,39] While a small change in the uptake of CTxB-MSNs was observed with both chemical and competitive inhibition of GM_1, a cell surface gangliosphingolipid know act as the primary receptor for the native toxin[34,40] this difference was not found to be significant. The intracellular behavior of CTxB-MSNs following uptake was carefully studied using laser scanning confocal microscopy. Due to the small size of the materials used in this study and the limited resolution of light microscopy, quantitative colocalization analysis was used to evaluate the statistical relevance of observed colocalization with cellular organelles. Unlike the two control materials used in this study (MSNs and PEGC-MSNs), CTxB-MSNs were found to exhibit significantly reduced colocalization with cellular lysosomes in a similar fashion to the native protein. CTxB-modified MSNs were also found to exhibit higher average colocalization with the golgi apparatus over control materials although no significant difference in the propensity of these materials to localize to the endoplasmic reticulum was observed. Using CTxB-MSNs to mediate the delivery of the membrane impermeable fluorophore propidium iodide did, however, provide evidence of localization to the endoplasmic reticulum as only localization to this organelle could result in the release of loaded PI and nuclear staining. From this, it can be concluded that CTxB-MSNs do appear capable of evading incorporation into lysosomes and localizing to the other cellular structures investigated in this work, presumably by the same mechanism used by the native protein.

In conclusion, from the investigations carried out in this work it could be determined that modification of MSNs with CTxB can alter the behavior and improve the efficacy of delivery of these materials. In comparison to the unmodified control materials, it was evident that CTxB did influence the internalization and intracellular behavior of

MSNs; shifting uptake toward CAVME, depressing lysosomal colocaliztion, and increasing the propensity of these materials to localize in the golgi apparatus and endoplasmic reticulum. From these observations it would be reasonable to suppose that CTxB bound to MSNs was mediating the intracellular trafficking of these materials, directing them through the golgi apparatus and presumably to the endoplasmic reticulum in a manner similar to that of the native protein. That these materials could deliver propidium iodide to the endoplasmic reticulum further supported the possibility of retrograde intracellular trafficking by CTxB-modified MSNs. While the effect of conjugated CTxB on nanoparticle behavior was evident throughout this work, attempts to evaluate its impact were complicated by the fact that the observed effects on the behavior of the material were often small. From this, it may be inferred that only a small fraction of CTxB-MSNs are capable of retrograde trafficking to the endoplasmic reticulum, with the majority appearing to be incapable of doing so. One possible cause of this limitation could be the lack of control exhibited by the coupling chemistry used to mediate the conjugation of the protein to the material surface. Improper conjugation could potentially result in the protein being bound in an orientation that occluded its binding site or altered its activity.[41] In order to eliminate variability in the behavior of CTxB-modified materials, alternative bioconjugation methods permitting greater control over the orientation of the bound protein would have to be employed. One possible bioconjugation strategy that would reduce variation in protein binding would be to use a copper(I)-catalyzed cycloaddition to mediate the attachment of a protein bearing a unnatural amino acid with an azide side-chain and a terminal alkyne.[42] A simple modification of the

PEGC linker used in this work would make this approach feasible for our MSN materials (Scheme 3).

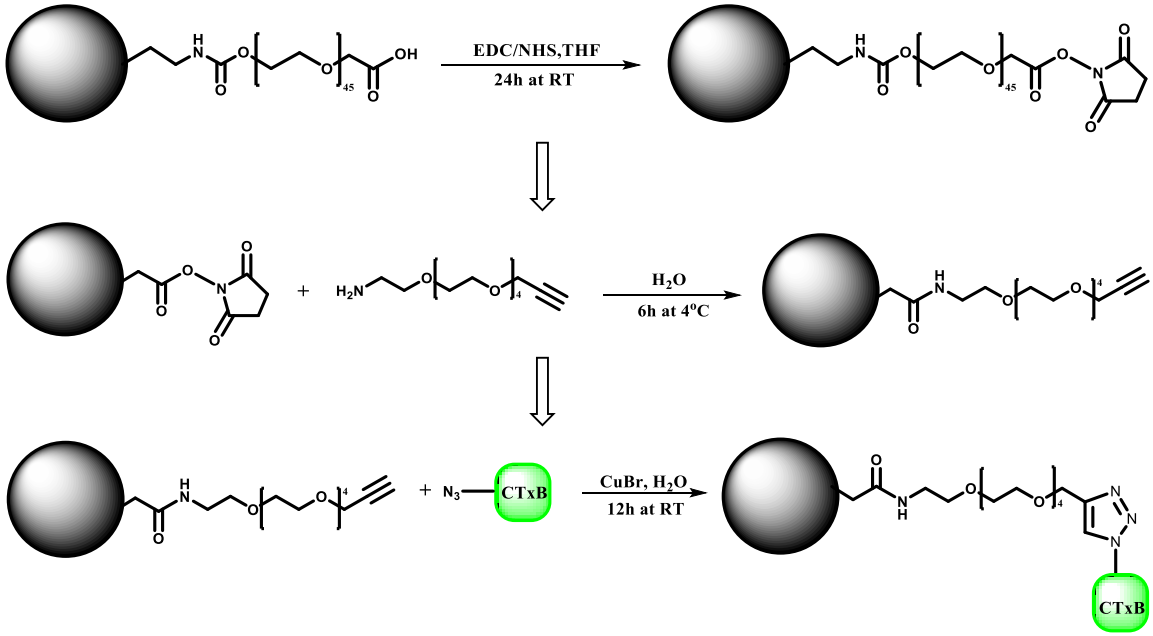

Scheme 3. Three-step hypothetical procedure for the controlled biocojugation of CTxB to MSNs.

Another possible limiter of CTxB-MSN behavior was proposed by Tekle et al. in their work on the intracellular behavior of quantum dots conjugated to the B subunits of shiga and ricin toxin. Here, they proposed the size of their quantum dot ligands (30-50nm) as a possible cause of the absence of retrograde trafficking in their materials.[41] While not addressed in this work, the effect of material size on the behavior bioconjugated nanoparticles remains an important question that will have to be answered before a comprehensive understanding of these materials can be reached. In addition to these considerations, future efforts to understand the intracellular behavior of MSNs and other bioconjugated nanomaterials would be aided by higher resolution imaging methods unavailable for use in this work such as biological TEM. The resolving power of these imaging techniques would help to overcome the ambiguity in material intracellular

localization arising from the limitations of the instruments used in this work. As it stands, conjugation of CTxB remains a promising approach for controlling the intracellular behavior of nanoparticles. This demonstrates in the most limited fashion the possibility of using bioactive macromolecules to modulate the interactions of nanocarriers with their cellular targets. While many challenging questions remain to be resolved in this growing field of biological nanoscience, in no way does this diminish the interesting possibilities that may be realized through this approach.

REFERENCES

1. Fadeel, B.; Garcia-Bennett, A. E., Better safe than sorry: Understanding the toxicological properties of inorganic nanoparticles manufactured for biomedical applications. *Advanced Drug Delivery Reviews* **2010,** *62* (3), 362-374.

2. Slowing, II; Vivero-Escoto, J. L.; Wu, C. W.; Lin, V. S. Y., Mesoporous silica nanoparticles as controlled release drug delivery and gene transfection carriers. *Advanced Drug Delivery Reviews* **2008,** *60* (11), 1278-1288.

3. Mura, S.; Nicolas, J.; Couvreur, P., Stimuli-responsive nanocarriers for drug delivery. *Nature Materials* **2013,** *12* (11), 991-1003.

4. Sahay, G.; Alakhova, D. Y.; Kabanov, A. V., Endocytosis of nanomedicines. *Journal of Controlled Release* **2010,** *145* (3), 182-195.

5. Kraft, J. C.; Freeling, J. P.; Wang, Z.; Ho, R. J. Y., Emerging Research and Clinical Development Trends of Liposome and Lipid Nanoparticle Drug Delivery Systems. *Journal of Pharmaceutical Sciences* **2014,** *103* (1), 29-52.

6. Arouri, A.; Hansen, A. H.; Rasmussen, T. E.; Mouritsen, O. G., Lipases, liposomes and lipid-prodrugs. *Current Opinion in Colloid & Interface Science* **2013,** *18* (5), 419-431.

7. Chou, L. Y. T.; Ming, K.; Chan, W. C. W., Strategies for the intracellular delivery of nanoparticles. *Chemical Society Reviews* **2011,** *40* (1), 233-245.

8. Vivero-Escoto, J. L.; Slowing, II; Trewyn, B. G.; Lin, V. S. Y., Mesoporous Silica Nanoparticles for Intracellular Controlled Drug Delivery. *Small* **2010,** *6* (18), 1952-1967.

9. Vercauteren, D.; Rejman, J.; Martens, T. F.; Demeester, J.; De Smedt, S. C.; Braeckmans, K., On the cellular processing of non-viral nanomedicines for nucleic acid delivery: Mechanisms and methods. *Journal of Controlled Release* **2012,** *161* (2), 566-581.

10. Rajendran, L.; Knolker, H. J.; Simons, K., Subcellular targeting strategies for drug design and delivery. *Nature Reviews Drug Discovery* **2010,** *9* (1), 29-42.

11. Kumari, S.; Swetha, M. G.; Mayor, S., Endocytosis unplugged: multiple ways to enter the cell. *Cell Research* **2010,** *20* (3), 256-275.

12. Doherty, G. J.; McMahon, H. T., Mechanisms of Endocytosis. *Annual Review of Biochemistry* **2009,** *78*, 857-902.

13. Bhuin, T.; Roy, J. K., Rab proteins: The key regulators of intracellular vesicle transport. *Experimental Cell Research* **2014,** *328* (1), 1-19.

14. Pfeffer, S. R., Unsolved mysteries in membrane traffic. *Annual Review of Biochemistry* **2007,** *76*, 629-645.

15. Petros, R. A.; DeSimone, J. M., Strategies in the design of nanoparticles for therapeutic applications. *Nature Reviews Drug Discovery* **2010,** *9* (8), 615-627.

16. Gruenberg, J.; van der Goot, F. G., Mechanisms of pathogen entry through the endosomal compartments. *Nature Reviews Molecular Cell Biology* **2006,** *7* (7), 495-504.

17. Herd, H. L.; Malugin, A.; Ghandehari, H., Silica nanoconstruct cellular toleration threshold in vitro. *Journal of Controlled Release* **2011,** *153* (1), 40-48

18. Shete, H. K.; Prabhu, R. H.; Patravale, V. B., Endosomal Escape: A Bottleneck in Intracellular Delivery. *Journal of Nanoscience and Nanotechnology* **2014,** *14* (1), 460-474.

19. Medina-Kauwe, L. K., "Alternative" endocytic mechanisms exploited by pathogens: New avenues for therapeutic delivery? *Advanced Drug Delivery Reviews* **2007,** *59* (8), 798-809;

20. Tarrago-Trani, M. T.; Storrie, B., Alternate routes for drug delivery to the cell interior: Pathways to the Golgi apparatus and endoplasmic reticulum. *Advanced Drug Delivery Reviews* **2007,** *59* (8), 782-797.

21. Odumosu, O.; Nicholas, D.; Yano, H.; Langridge, W., AB Toxins: A Paradigm Switch from Deadly to Desirable. *Toxins* **2010,** *2* (7), 1612-1645.

22. Paulo, C. S. O.; das Neves, R. P.; Ferreira, L. S., Nanoparticles for intracellular-targeted drug delivery. *Nanotechnology* **2011,** *22* (49).

23. Chakraborty, S. K.; Fitzpatrick, J. A. J.; Phillippi, J. A.; Andreko, S.; Waggoner, A. S.; Bruchez, M. P.; Ballou, B., Cholera toxin B conjugated quantum dots for live cell Labeling. *Nano Letters* **2007,** *7* (9), 2618-2626.

24. Qiao, Z.-A.; Zhang, L.; Guo, M.; Liu, Y.; Huo, Q., Synthesis of Mesoporous Silica Nanoparticles via Controlled Hydrolysis and Condensation of Silicon Alkoxide. *Chemistry of Materials* **2009,** *21* (16), 3823-3829.

25. Warnecke, A.; Kratz, F., Maleimide-oligo(ethylene glycol) derivatives of camptothecin as albumin-binding prodrugs: Synthesis and antitumor efficacy. *Bioconjugate Chemistry* **2003,** *14* (2), 377-387.

26. Pollock, S.; Antrobus, R.; Newton, L.; Kampa, B.; Rossa, J.; Latham, S.; Nichita, N. B.; Dwek, R. A.; Zitzmann, N., Uptake and trafficking of liposomes to the endoplasmic reticulum. *Faseb Journal* **2010,** *24* (6), 1866-1878.

27. Bolte, S.; Cordelieres, F. P.: A guided tour into subcellular colocalization analysis in light microscopy. *J. Microsc.* **2006**, *224*, 213-232.

28. Davies, S. P.; Reddy, H.; Caivano, M.; Cohen, P., Specificity and mechanism of action of some commonly used protein kinase inhibitors. *Biochemical Journal* **2000,** *351*, 95-105.

29. De Haes, W.; Van Mol, G.; Merlin, C.; De Smedt, S. C.; Vanham, G.; Rejman, J., Internalization of mRNA Lipoplexes by Dendritic Cells. *Molecular Pharmaceutics* **2012,** *9* (10), 2942-2949.

30. Jambhrunkar, S.; Qu, Z.; Popat, A.; Yang, J.; Noonan, O.; Acauan, L.; Nor, Y. A.; Yu, C.; Karmakar, S., Effect of Surface Functionality of Silica Nanoparticles on Cellular Uptake and Cytotoxicity. *Molecular Pharmaceutics* **2014,** *11* (10), 3642-3655

31. Hao, N.; Li, L.; Zhang, Q.; Huang, X.; Meng, X.; Zhang, Y.; Chen, D.; Tang, F.; Li, L., The shape effect of PEGylated mesoporous silica nanoparticles on cellular uptake pathway in Hela cells. *Microporous and Mesoporous Materials* **2012,** *162*, 14-23.

32. Vercauteren, D.; Vandenbroucke, R. E.; Jones, A. T.; Rejman, J.; Demeester, J.; De Smedt, S. C.; Sanders, N. N.; Braeckmans, K., The Use of Inhibitors to Study Endocytic Pathways of Gene Carriers: Optimization and Pitfalls. *Molecular Therapy* **2010,** *18* (3), 561-569.

33. Stuart, E. S.; Webley, W. C.; Norkin, L. C., Lipid rafts, caveolae, caveolin-1, and entry by Chlamydiae into host cells. *Experimental Cell Research* **2003,** *287* (1), 67-78.

34. Fujinaga, Y.; Wolf, A. A.; Rodighiero, C.; Wheeler, H.; Tsai, B.; Allen, L.; Jobling, M. G.; Rapoport, T.; Holmes, R. K.; Lencer, W. I., Gangliosides that associate with lipid rafts mediate transport of cholera and related toxins from the plasma membrane to endoplasmic reticulm. *Molecular Biology of the Cell* **2003,** *14* (12), 4783-4793.

35. Lee, L.; Abe, A.; Shayman, J. A., Improved inhibitors of glucosylceramide synthase. *Journal of Biological Chemistry* **1999,** *274* (21), 14662-14669.

36. Haicheur, N.; Benchetrit, F.; Amessou, M.; Leclerc, C.; Falguieres, T.; Fayolle, C.; Bismuth, E.; Fridman, W. H.; Johannes, L.; Tartour, E., The B subunit of Shiga toxin coupled to full-size antigenic protein elicits humoral and cell-mediated immune

responses associated with a T(h)1-dominant polarization. *International Immunology* **2003,** *15* (10), 1161-1171.

37. Moore, A.; Donahue, C. J.; Bauer, K. D.; Mather, J. P., Simultaneous measurement of cell cycle and apoptotic cell death. *Methods Cell Biol* **1998,** *57*, 265-78.

38. Wernick, N. L. B.; Chinnapen, D. J. F.; Cho, J. A.; Lencer, W. I., Cholera Toxin: An Intracellular Journey into the Cytosol by Way of the Endoplasmic Reticulum. *Toxins* **2010,** *2* (3), 310-325.

39. Payne, C. K.; Jones, S. A.; Chen, C.; Zhuang, X. W., Internalization and trafficking of cell surface proteoglycans and proteoglycan-binding ligands. *Traffic* **2007,** *8* (4), 389-401.

40. Watson, P.; Spooner, R. A., Toxin entry and trafficking in mammalian cells. *Advanced Drug Delivery Reviews* **2006,** *58* (15), 1581-1596.

41. Tekle, C.; van Deurs, B.; Sandvig, K.; Iversen, T. G., Cellular trafficking of quantum dot-ligand bioconjugates and their induction of changes in normal routing of unconjugated ligands. *Nano Letters* **2008,** *8* (7), 1858-1865.

42. Wang, Q.; Chan, T. R.; Hilgraf, R.; Fokin, V. V.; Sharpless, K. B.; Finn, M. G., Bioconjugation by copper(I)-catalyzed azide-alkyne 3+2 cycloaddition. *Journal of the American Chemical Society* **2003,** *125* (11), 3192-3193.

APPENDIX A: MATERIAL CYTOTOXICITY ASSAYS

This appendix contains cell viability curves for all materials used in the preceding work. Total cell viability was determined using the same procedure that was used to quantify cytotoxicity of MSN-mediated protein delivery.

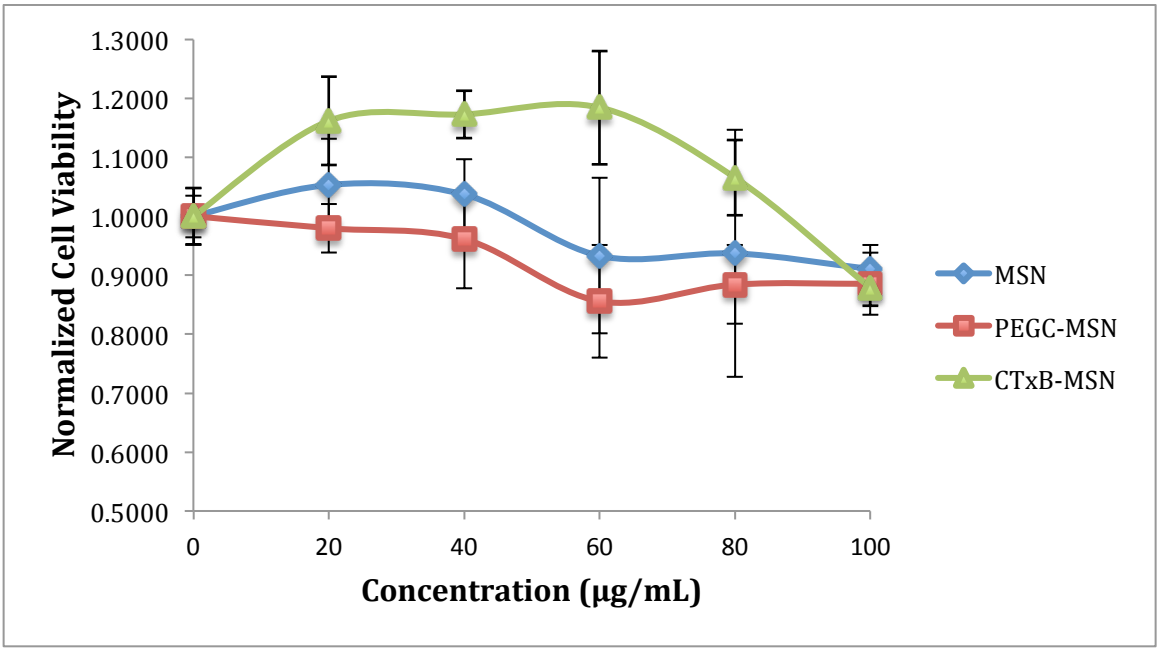

Figure A1. MSN, PEGC-MSN, and CTxB-MSN material cytotoxicity 24 hours post-inoculation.

APPENDIX B: SUPPLEMENTAL CONFOCAL IMAGES

These appendixes contain additional Laser Scanning Confocal Microscopy images for organelle colocalization and PI uptake/release. Three additional images are supplied for all materials for each of the conditions investigated in this work.

LYSOSOMAL COLOCALIZATION

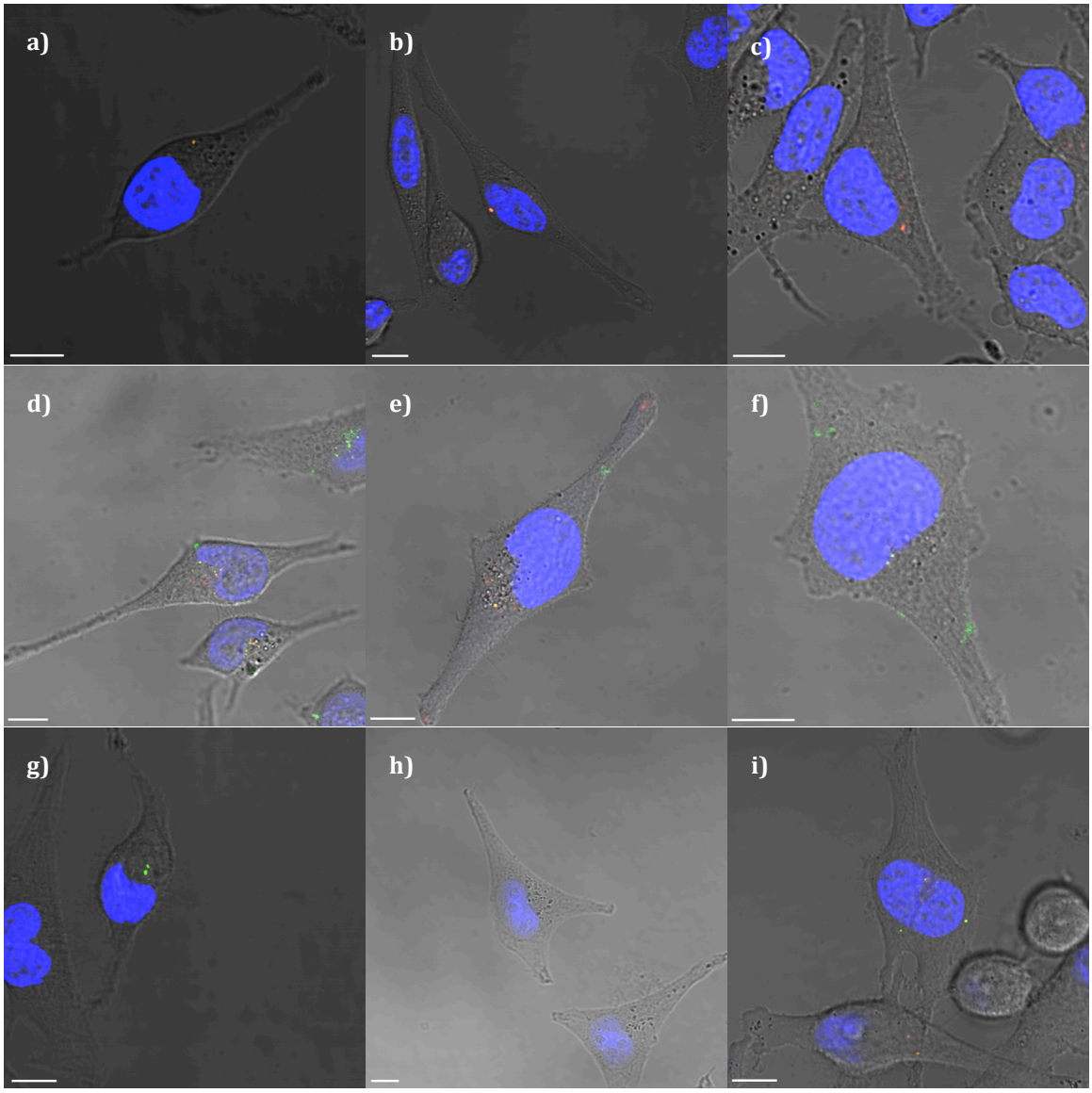

Figure B1. Lysosomal colocalization of MSN (a,b,c), PEGC-MSN(d,e,f), and CTxB-MSN(g,h,i). All the scale bars are 10 μm in size.

APPENDIX B: (Continued)

GOLGI APPARATUS COLOCALIZATION

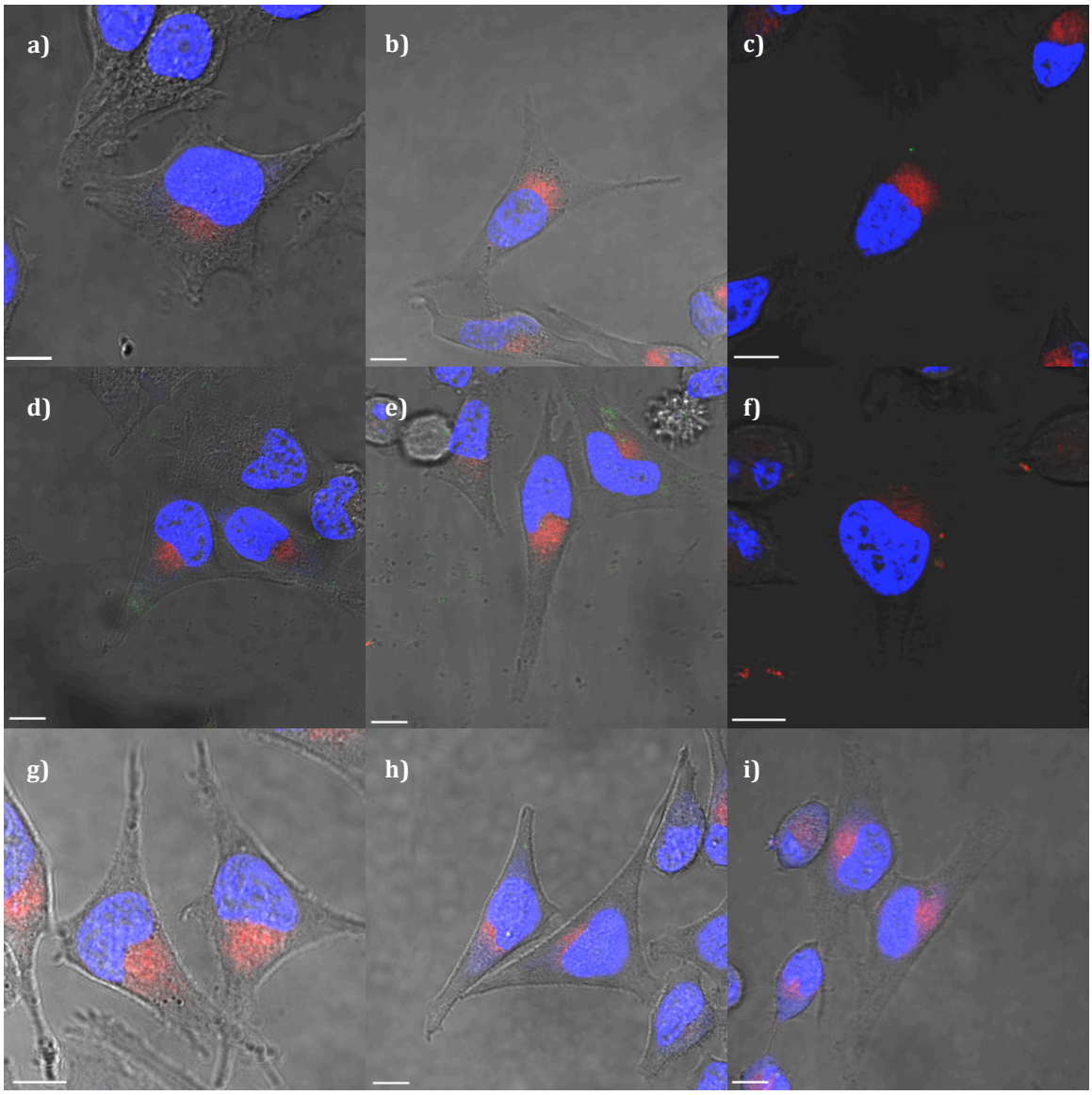

Figure B2.Gogli apparatus colocalization of MSN(a,b,c), PEGC-MSN(d,e,f), and CTxB-MSN(g,h,i). All the scale bars are 10 μm in size.

APPENDIX B: (Continued)

ENDOPLASMIC RETICULUM COLOCALIZATION

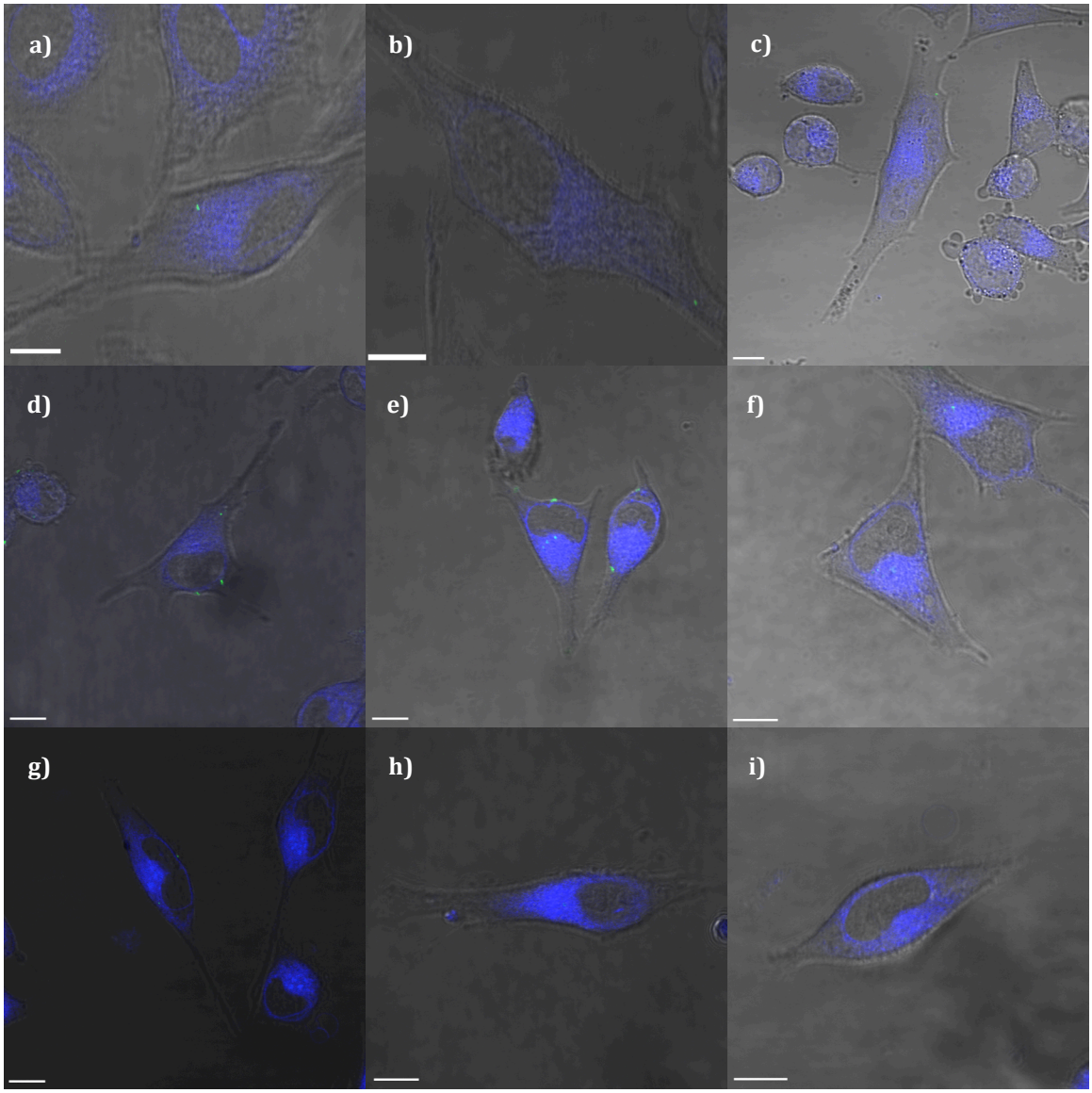

Figure B3.Endoplasmic reticulum colocalization of MSN(a,b,c), PEGC-MSN(d,e,f), and CTxB-MSN(g,h,i). All the scale bars are 10 μm in size.

APPENDIX B: (Continued)

ENDOPLASMIC RETICULUM VS. LYSOSOMAL COLOCALIZATION

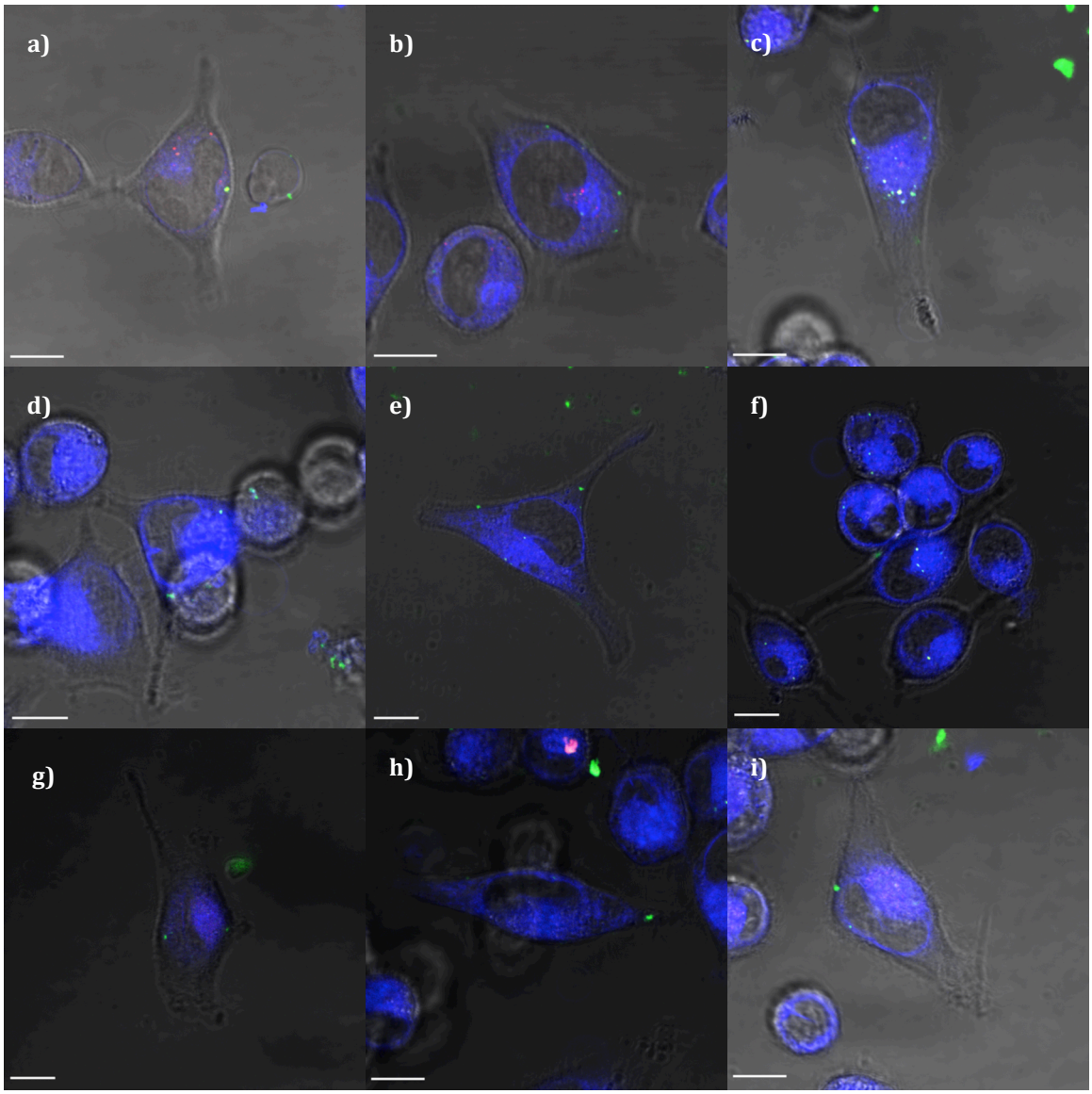

Figure B4. Relative colocalization of MSN(a,b,c), PEGC-MSN(d,e,f), and CTxB-MSN(g,h,i) in ER and lysosomes. All the scale bars are 10 μm in size.

APPENDIX B: (Continued)

PROPIDIUM IODIDE RELEASE

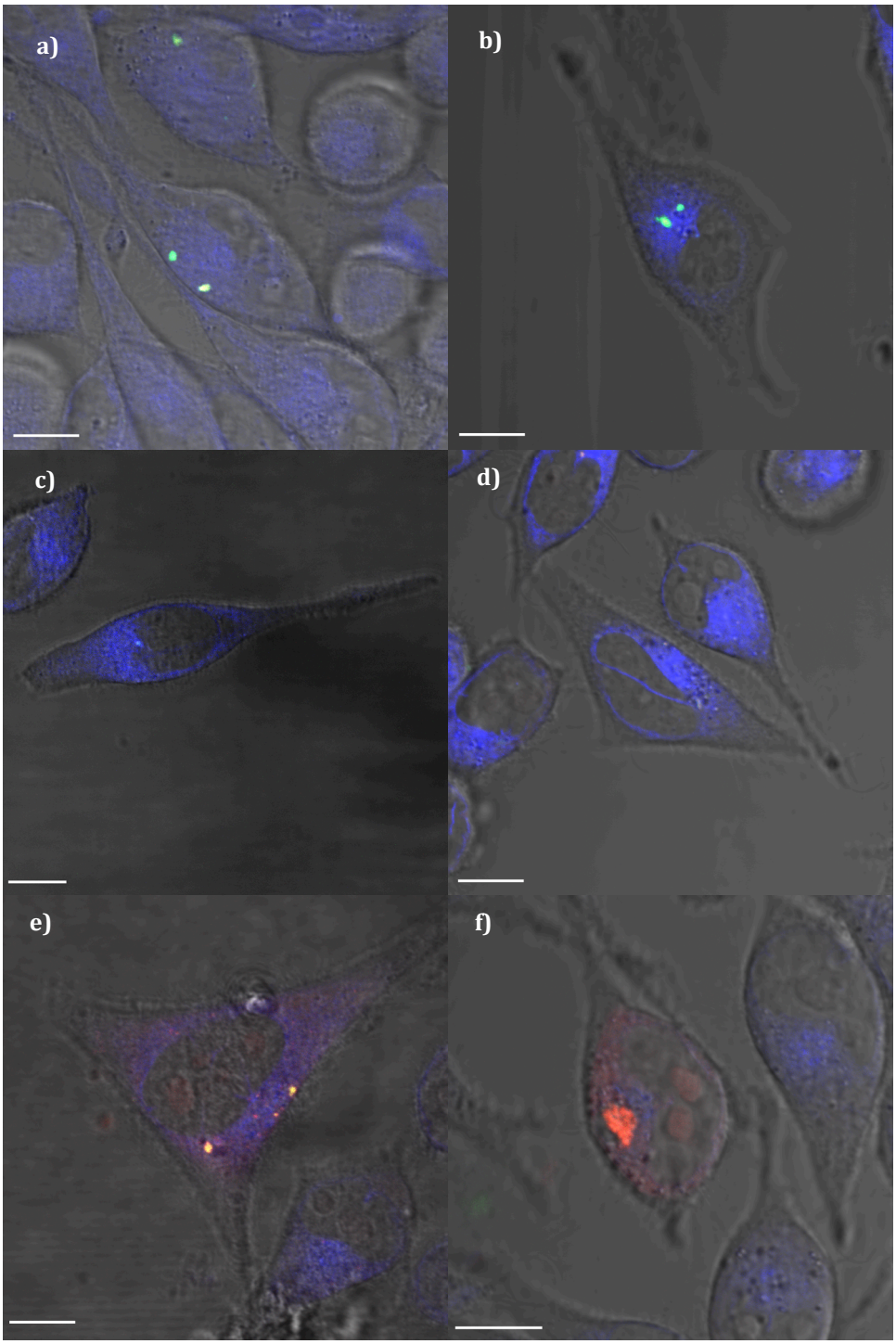

Figure B5. Intracellular delivery and release of PI mediated by MSNs (a,b), PEGC-MSNs (c,d), and CTxB-MSNs (e,f). All the scale bars are 10 μm in size.